

Montana Tech Library

Digital Commons @ Montana Tech

Graduate Theses & Non-Theses

Student Scholarship

Spring 2021

**Comparison of Pore Water Chemistry Between an Upland
Restoration Site and a Valley Superfund Site Using Inorganic
Carbon Isotopes Along Blacktail Creek, Butte, MT**

Kyle Nacey

Follow this and additional works at: https://digitalcommons.mtech.edu/grad_rsch

Comparison of Pore Water Chemistry Between an Upland Restoration Site
and a Valley Superfund Site Using Inorganic Carbon Isotopes Along
Blacktail Creek, Butte, MT

by
Kyle Nacey

A thesis submitted in partial fulfillment of the
requirements for the degree of

Master of Science: Geoscience
Geology option

Montana Tech
2021



Abstract

Three sites were chosen along Blacktail creek to compare sediment pore water chemistry. The sites were chosen to reflect a valley superfund site, a Beaver Mimicry Structure (BMS) restoration site, and a wetland with a natural/historical beaver dam. Sediment pore water diffusion samplers (peepers) were deployed in each of the three sites to sample metals, dissolved inorganic carbon, $\delta^{13}\text{C}$ isotopes, alkalinity, and major anions. Data sets from the peepers were used to determine microbial process that influence the geochemistry of the creek with regard to trace metals and DIC. A wetland (historical) site displayed $\delta^{13}\text{C}$ ratios and DIC concentrations consistent with acetoclastic methanogenesis which converts acetate to isotopically enriched CO_2 and isotopically depleted CH_4 . The beaver mimicry restoration site (BMS) site sees aerobic respiration producing DIC in Blacktail creek. The BMS site also sees a 5 cm layer where Fe and Mn oxide reduction is taking place, this is indicated by a large increase in dissolved Fe, Mn, As, and P. The downstream peeper displayed methanogenesis, Fe/Mn oxide reduction, and bacterial sulfate reduction. Dissolved Fe and Mn increase more than tenfold in the sediment and there is also a corresponding spike in As and P. These processes can be identified by comparing the concentration of DIC in the sediment to the $\delta^{13}\text{C}$ isotopic value, as well as Fe, Mn, As, and P.

Keywords: Butte, DIC, carbon, flux, Beaver mimicry

Dedication

Knowledge speaks, but wisdom listens. -Jimi Hendrix.

Acknowledgements

I would like to thank Dr. Glenn Shaw and Dr. Chris Gammons for helping me come up with a project that fits my interests as well as their guidance through every aspect of this project. Analytical work conducted by Jackie Timmer and Ashley Huft at the Montana Bureau of Mines and Geology. A special thank you to Jackie Timmer for helping me run the carbon analyzer. Funding for this project was provided by Montana Tech Geological Engineering Department, Montana Tech Graduate Research Office, Montana Natural Resource Damage Program (MNRDP), and the Butte Natural Resource Council (BNRC).

Committee members: Dr. Glenn Shaw-advisor Department of Geological Engineering, Dr. Chris Gammons- co-advisor Department of Geological Engineering, Jackie Timmer-MBMG Chief Analytical Chemist, Dr. Bev Hartline-Vice Chancellor of Research

Table of Contents

ABSTRACT	I
DEDICATION	II
ACKNOWLEDGEMENTS	III
LIST OF TABLES	VII
LIST OF FIGURES.....	IX
LIST OF EQUATIONS	XI
GLOSSARY OF TERMS.....	XIII
1. INTRODUCTION AND BACKGROUND KNOWLEDGE.....	1
1.1. <i>Locations</i>	6
1.2. <i>Previous Studies</i>	8
1.3. <i>Scope of project</i>	14
1.4. <i>Hypothesis and research questions</i>	15
2. METHODOLOGY	16
2.1. <i>Field Methods</i>	16
2.2. <i>Peeper preparation, deployment, and sampling</i>	17
2.3. <i>Analytical Methods</i>	20
2.3.1. Dissolved inorganic carbon (DIC).....	20
2.3.2. ICP-MS and ICP-OES	21
2.3.3. Ion Chromatography	22
2.4. <i>Sediment cores</i>	22
2.5. <i>Equations and Calculations</i>	22
2.5.1. Estimating pH	22
2.5.2. Calculating flux for metals and DIC.....	24
2.5.3. Partitioning inorganic carbon isotopes between H_2CO_3 and HCO_3^-	25

3. RESULTS.....	28
3.1. Lower Blacktail Creek (Peepers 18 and 19)	28
3.1.1. Speciating DIC.....	32
3.1.2. DIC isotope partitions.....	33
3.1.3. Sediment core	33
3.1.4. Estimated pH	33
3.1.4.1. Diffusive flux in the downstream site.....	35
3.2. Upper Blacktail Recently Deposited Sediment (Peepers 20 and 21).....	35
3.2.1. Sediment core	38
3.2.2. Calculated pH	39
3.2.3. Peeper 20 DIC speciation.....	40
3.2.4. DIC isotope partitions.....	41
3.2.4.1. Diffusive flux in the BMS site	42
3.3. Upper Blacktail Creek in Pond Sediments (Peeper 22 and 23)	43
3.3.1. Sediment	44
3.3.2. Calculated pH	45
3.3.3. DIC speciation.....	46
3.3.4. DIC isotope partitions.....	47
3.3.4.1. Diffusive flux in the historical site	48
3.4. Surface water of Blacktail Creek in between the three sites	48
4. DISCUSSION AND IMPLICATIONS.....	51
4.1. Microbial reactions	51
4.1.1. Aerobic respiration.....	52
4.1.2. Denitrification and Dissimilatory nitrate reduction to ammonia	53
4.1.3. Iron and Manganese oxide reduction	54
4.1.4. Sulfate reduction.....	55
4.1.5. Fermentation (methanogenesis).....	58
4.2. Interactions within the BMS site	59

4.3.	<i>Tracking DIC between the BMS site and the downstream site</i>	63
4.4.	<i>Predicting microbial processes based on surface DIC</i>	65
5.	CONCLUSIONS AND RECOMMENDATIONS	67
5.1.	<i>Conclusions</i>	67
5.2.	<i>Future work</i>	68
6.	REFERENCES	69
7.	APPENDIX A: PEEPER SAMPLING PLANS	77
8.	APPENDIX B: DIC RESULTS BY PEEPER	80
9.	APPENDIX C: ION CHROMATOGRAPHY	83
10.	APPENDIX D: ICP-OES AND ICP-MS	84
11.	APPENDIX E: SURFACE WATER DATA	91
12.	APPENDIX F: GROUNDWATER WELLS	92
13.	APPENDIX G: SURFACE WATER FIELD PHOTOS	93

List of Tables

Table I: General peeper layout of each of the three sets of peepers	19
Table II: Diffusive flux constants where units of D_0 are ($\mu\text{g sec}^{-1} \text{cm}^{-2}$)	25
Table III: Sampling dates for peepers, groundwater, and surface water	28
Table IV: Calculated pH of peepers 18 and 19.....	34
Table V: Diffusive flux in peeper 18	35
Table VI: calculated pH values for peepers 20 and 21	39
Table VII: Peeper 20 diffusive flux	42
Table VIII: Calculated pH for peepers 22 and 23.....	45
Table IX: peeper 23 diffusive flux.....	48
Table X: Surface water chemistry.....	50
Table XI: Peeper 20 and 21 sampling layout.....	77
Table XII: Peeper 18 and 19 sampling layout	78
Table XIII: Peeper 22-23 sampling layout.....	79
Table XIV: Peeper 18 and 19 results corrected for dilution	80
Table XV: peeper 20 and 21 DIC results, corrected for dilution.....	81
Table XVI: Peeper 22 and 23 DIC and alkalinity results, corrected for dilution	82
Table XVII: Ion Chromatography peeper 18 and 19, corrected for dilution	83
Table XVIII: Peeper 20 and 21 Ion Chromatography results, corrected for dilution	84
Table XIX: Peeper 18 and 19 ICP-OES, corrected for dilution	84
Table XX: Peeper 20 and 21 ICP-OES, corrected for dilution.....	85
Table XXI: peeper 22 and 23 ICP-OES results, corrected for dilution	86
Table XXII: Peeper 20 and 21 ICP-MS results, corrected for dilution	87

Table XXIII: Peeper 20 and 21 ICP-MS results, corrected for dilution cont.	88
Table XXIV: Peepers 18 and 19 ICP-MS results corrected for dilution	89
Table XXV: Peepers 18 and 19 ICP-MS, results corrected for dilution cont.	90
Table XXVI: Surface water samples between sites (September 18 th , 2020)	91

List of Figures

Figure 1: Location map of Butte, MT, and the study sites	7
Figure 2: Example of a beaver mimicry structure in the BMS site	9
Figure 3: Peepers 20 and 21 in the sediment (left) sediment core (right).....	10
Figure 4: Peepers in older sediment in the historical site	12
Figure 5: Downstream peeper 18 site in the Butte superfund site	13
Figure 6: Peeper setup, left is peeper sets, right (Rader, 2019) is peeper schematic	17
Figure 7: $\log fO_2$ vs pH (left) and Bjerrum plot of inorganic carbon (right)	23
Figure 8: Diagram from (Clark and Fritz, 1997) showing isotopic equilibrium	27
Figure 9: Peeper 18 results.....	29
Figure 10: Peeper 18 downstream results for P, NO_3^- , and SO_4^{2-} , NO_3^-	30
Figure 11: Iron speciation diagram.....	31
Figure 12: Difference between DIC and Alkalinity shows H_2CO_3	32
Figure 13: $\delta^{13}C$ Isotope partitions in Peeper 18.....	33
Figure 14: Peepers 20 and 21 results	36
Figure 15: Peepers 20 and 21 results	37
Figure 16: Sediment core from peepers 20 and 21	38
Figure 17: Filtered DIC in peeper 20.....	40
Figure 18: $\delta^{13}C$ isotope partitions in the BMS site	41
Figure 19: Peeper 22 and 23 results, 0 indicates SWI, note variance in X axes.....	43
Figure 20: Iron oxide precipitation in historical site sample	44
Figure 21: Peeper 23 DIC speciation in historical site	46
Figure 22: Isotopic compositions of DIC in peeper 23.....	47

Figure 23: Map of surface water samples in between peeper sites.....	49
Figure 24: Sulfur speciation diagram at stream conditions (Dick, 2019).....	56
Figure 25: SO_4^{2-} , F^- , and Cl^- concentrations with depth in peeper 18	57
Figure 26: DIC and DIC isotopes for peeper 18.....	58
Figure 27: The local meteoric water line for Southwest Montana.....	60
Figure 28: Endmember mixing plot of the BMS site based on inverse DIC	62
Figure 29: DIC concentrations with distance downstream from BMS site.	65
Figure 30: Groundwater wells in BMS site Stemp_3 (left) and SW_UFLCW (right).	92
Figure 31: Groundwater well sampled in BMS site Stemp_1	92
Figure 32: BTC-6 surface water site.....	93
Figure 33: BTC-7 Surface water site	94
Figure 34: BTC-8 surface water site.....	95
Figure 35: BTC-3 surface water site.....	96
Figure 36: BTC-4 surface water site.....	97

List of Equations

Equation 1	2
Equation 2	11
Equation 3	20
Equation 4	22
Equation 5	23
Equation 6	24
Equation 7	24
Equation 8	25
Equation 9	25
Equation 10	26
Equation 11	26
Equation 12	26
Equation 13	26
Equation 14	52
Equation 15	53
Equation 16	53
Equation 17	53
Equation 18	54
Equation 19	54
Equation 20	54
Equation 21	55
Equation 22	56

Equation 23	57
Equation 24	57
Equation 25	57

Glossary of Terms

Term	Definition
μg/L	Microgram per liter
ALS	Aquatic life standard
As	Arsenic
BMSR	Beaver mimicry restoration
BMS	Beaver mimicry
BTC	Blacktail Creek
cfs	Cubic feet per second
δ ¹⁸ O/δD	Isotopic value of Oxygen and Deuterium
δ ¹³ C	Isotopic value of inorganic carbon
DIC	Dissolved inorganic carbon
DOC	Dissolved organic carbon
DNRA	Dissimilatory nitrate reduction to ammonium
DO	Dissolved oxygen
Cu	Copper
Eh	Redox potential
EPA	Environmental Protection Agency
Fe	Iron
Fe ²⁺	Ferrous iron
Fe ³⁺	Ferric iron
IC	Ion Chromatography
ICP-MS	Inductively coupled plasma-mass spectrometry
ICP-OES	Inductively coupled plasma-optical emission spectrometry
LAO	Lower Area One
MBMG	Montana Bureau of Mines and Geology
mg/kg	Milligram per kilogram
mg/L	Milligram per liter
Mn	Manganese
NOAA	National Oceanic and Atmospheric Administration
ORP	Oxidation reduction potential
Peeper	Sediment pore water sampler
ppb	Parts per billion
ppm	Parts per million
pH	-log α[H ⁺]
SBC	Silver Bow Creek
SC	Specific Conductivity
SRB	Sulfate reducing bacteria
SWI	Sediment water interface
T	Temperature (C°)
Zn	Zinc

1. Introduction and background knowledge

The following information is paraphrased from Eby (2016). Atmospheric carbon is the dominant source of carbon in almost all open water and aquatic environments. There are many different modes of transport for carbon. The study of these processes is referred to as carbon cycling. Carbon cycling moves carbon from one place to another in the form of sources and sinks; it can be used by organisms, dissolved into water, transformed into other forms of organic or inorganic carbon, and/or released back into the atmosphere. Organic (reduced) carbon has more electrons available for reactions and inorganic (oxidized) carbon has fewer electrons available. When inorganic carbon is reduced via redox reactions, such as photosynthesis, it is referred to as carbon fixation. Carbon fixation is an important aspect in the process of converting inorganic carbon ($\text{CO}_2(g)$, $\text{CO}_2(aq)$, $\text{H}_2\text{CO}_3(aq)$, $\text{HCO}_3^-(aq)$, $\text{CO}_3^{2-}(aq)$, $\text{CaCO}_3(s)$, note that $\text{CO}_2(aq)$ and $\text{H}_2\text{CO}_3(aq)$ are the same when dissolved in water) into organic carbon that can be used by organisms or converted to organic acids and ligands. Inorganic carbon species is pH dependent, which means there can be more H_2CO_3 than HCO_3^- , or vice versa depending on the pH constraints. One example of inorganic carbon fixation would be marine, lacustrine, and fluvial organisms using dissolved $\text{CO}_2(aq)$ and $\text{Ca}^{2+}(aq)$ and converting it to $\text{CaCO}_3(cr)$ for creating their own shells. When the organism dies, it releases the used carbon back into the water where it can be recycled again.

Atmospheric carbon is the most dominant source of CO_2 in open aquatic systems. The shell example above is an example of a carbon sink and could be quantified by calculating flux using Fick's law and equilibrium concentrations. Sinks remove overall inorganic carbon from the atmosphere. Tracking the sources and sinks of carbon can be a useful indicator of other hydrologic and biological processes that may exist in any given system.

Carbon has two stable isotopes and one radioactive isotope. ^{12}C , ^{13}C , ^{14}C with ^{14}C being the radioactive isotope. Relative abundances are as follows: 98.89%, 1.11% and $<0.10\%$ respectively. Special instrumentation is required to measure ^{14}C . While the percentage of ^{13}C is small compared to ^{12}C , the fraction of $^{13}\text{C}/^{12}\text{C}$ is useful to understand certain hydrogeochemical processes.

In most cases, when inorganic carbon is converted, fixated, or simply moved from one location to another, a stable isotope fractionation may occur between ^{12}C and ^{13}C . With ^{12}C being one atomic mass unit (amu) lighter, biological organisms prefer to use ^{12}C rather than ^{13}C . This is because it requires more metabolic energy to processes ^{13}C as opposed to ^{12}C . Carbon isotope ratios are commonly compared to the international reference standard known as the Vienna PeeDee Belemnite (VPDB). The VPDB has a $^{13}\text{C}/^{12}\text{C}$ ratio of 0.01123720. (1) shows how the VPDB is used to compare DIC samples:

$$\delta^{13}\text{C} = \left(\frac{\left(\frac{^{13}\text{C}}{^{12}\text{C}} \right)_{\text{sample}}}{\left(\frac{^{13}\text{C}}{^{12}\text{C}} \right)_{\text{standard}}} - 1 \right) \times 1000 \text{‰} \quad (1)$$

where the standard ratio of $^{13}\text{C}/^{12}\text{C}$ is the value of $^{13}\text{C}/^{12}\text{C}$ in the VPDB and the sample ratio of $^{13}\text{C}/^{12}\text{C}$ is the value obtained from the instrument. $\delta^{13}\text{C}$ close to zero represent no significant difference in isotope ratio while values farther away from zero represent stronger fractionations compared to the VPDB standard. Fractionations can transfer either direction, but more commonly become depleted (more negative) due to biological processes. The more negative values are referred to as depleted in ^{13}C because the ratio of ^{13}C to ^{12}C becomes less than the VPDB standard. More positive values are referred to as enriched.

$\text{CO}_2(g)$ in the atmosphere also has its own isotopic composition that is monitored by the National Oceanic and Atmospheric Administration (NOAA) and routinely updated. These measurements are usually taken from Mauna Loa in Hawaii and serves as a good atmospheric average because of its location in the middle of the pacific, this value can vary regionally. The burning of fossil fuels is a source of atmospheric $\text{CO}_2(g)$. Fossil fuels are extracted from the earth in the form of a mixture of multiple organic compounds (gasoline, kerosene, diesel, etc.). They are the result of decaying organic matter that has occurred throughout earth's geological history. As previously mentioned, organisms prefer to use ^{12}C rather than ^{13}C . This means that fossil fuels are a source of depleted organic carbon which results in depleted $\text{CO}_2(g)$ being released when it is burned. Over anthropogenic time this process has slowly altered the isotopic composition of $\text{CO}_2(g)$ in the atmosphere. According to NOAA, the current average isotopic composition of carbon in the atmosphere is -8.5‰ which is more depleted compared to 1990 when it was -7.8‰ (NOAA, 2021). This is direct evidence of $\text{CO}_2(g)$ that is sourced from the burning of fossil fuels.

While the ocean is the primary sink of atmospheric CO_2 , the ocean becomes more acidic with more CO_2 in the atmosphere. When atmospheric $\text{CO}_2(g)$ is dissolved in ocean water, it becomes $\text{H}_2\text{CO}_3(aq)$ which is carbonic acid. Carbonic acid is a diprotic acid with $\text{HCO}_3^-(aq)$ (bicarbonate) being the intermediate buffer and $\text{CO}_3^{2-}(aq)$ (carbonate) being the conjugate base of bicarbonate and the endmember of $\text{H}_2\text{CO}_3(aq)$. Bicarbonate plays a key role as the primary buffer in aquatic systems and is usually the only source of alkalinity (acid neutralizing potential). In most aquatic systems, alkalinity is primarily in the form of bicarbonate, but can also be influenced by phosphates and silicates. (The information up to this point was adapted from Eby (2016) in *Principles of Environmental Geochemistry*.)

Beaver mimicry is a relatively new method of preventing rapid stream bed erosion in creeks and drainages. Rapid stream bed erosion upstream in higher elevations can lead to high sediment loading and deposition downstream, creating a sink for DIC, trace elements, and other solutes. The sediment becomes sources of these solutes during baseflow. The goal of beaver mimicry is to reverse rapid stream incision by creating structures that have similar effects as natural beaver dams. Natural and artificial beaver dam structures both influence the stream by keeping the stream in line with a flood plain, and they dramatically reduce the effects of erosion and sediment deposition downstream. The deployment of beaver dam mimicry structures (BMS) can influence how sources and sinks of carbon interact. Groundwater and hydrogeochemical interactions can influence a stream's health. The flux of nonreactive (conservative) metals between the stream sediments and surface water in freshwater environments can be quantified by using Fick's law when a concentration gradient exists between the sediments and the stream.

The focus of this study is on carbon and metals in Blacktail Creek near Butte, MT from the headwaters to the confluence with Silver Bow Creek. Blacktail Creek is a sub-alpine stream that transitions into a valley stream in Silver Bow County near Butte, Montana. Historically, Blacktail Creek has been negatively affected by mining pollution and forestry clearcutting, since the mid-late 1800's (Koch *et al.*, 2017). The effects of these anthropogenic processes, such as heavy metal contamination, stream incision in the Highlands, and high sediment loading downstream in the valleys, continue to influence the hydrogeochemical systems of the creek (Tucci and Icopini, 2012; Gammons *et al.*, 2014; Tucci, 2014; Norman, 2019). While aqueous samples directly from the creek measure overall creek health with the aquatic life and drinking water standards, it does not reflect the chemistry of the pore water in the stream bed sediments which can be orders of magnitude higher. Trace elements, and other solutes of interest, often

adsorb to fine grain sediments which then disperse into the creek over time (Gammons *et al*, 2014). With high sediment loading sourced from upstream, fine grain sediments continue to deposit and create a source for solutes to be released later during snowmelt.

The headwaters of Blacktail Creek begin in the Highlands Mountain range near Butte, Montana. Water quality in the Highlands is generally considered clean, pristine, and not associated with metal or nutrient contamination (Norman, 2020). A neighboring stream draining the Highlands, Basin Creek, which serves as a drinking water supply for the city of Butte. Blacktail Creek runs through an active restoration site where attempts are being made to reconnect the creek with its historical floodplain by placing artificial beaver dams in the creek (Norman, 2020).

Blacktail Creek then flows downstream about 10 km into the valley through the city of Butte, MT. Butte, MT is home to EPA designated superfund sites, which are the negative result of porphyry copper mining (EPA, 2018). The superfund sites in Butte include the Berkeley Pit Lake, and the Lower Area One (LAO) site. The LAO superfund site is known for having contaminated groundwater from the Parrot tailings, Diggings East, Northside Tailings, and other sources of pollution contributing to contaminated stream sediments and surface water (Metesh & Madison, 2004; Tucci and Icopini, 2012; Tucci, 2014, EPA, 2018). Lower Blacktail Creek flows through the LAO site.

1.1. Locations

The first study area is in the Highland Mountain range, near Thompson Park, and sits at approximately 1980 m, with the highest peaks reaching over 3000 m. This study site will be referred to as the Beaver-Mimicry Structure (BMS) site, as it is located in a site that is undergoing restoration using BMS. Near the BMS site is a historical beaver dam, but the beavers have been over trapped and are no longer present in the area. This natural beaver dam site will be referred to as the historical site and sits at approximately 1990 m. The BMS site also has a natural historical beaver dam but prior to restoration, the dam washed out. The historical site is on the south fork of the Blacktail Creek watershed shown in the map in Figure 1. The historical site is primarily standing water with low rates of flow. The third site is located about 18 km downstream in Butte as shown in Figure 1. This will be referred to as the downstream site, and it sits at an elevation of about 1670 m. The purpose of this site, being a low valley stream, is to compare the pore water chemistry of the superfund sediments, which have been known to have high concentrations of heavy metals (Tucci and Icopini, 2012; Tucci, 2014). All three sites were sampled during baseflow.

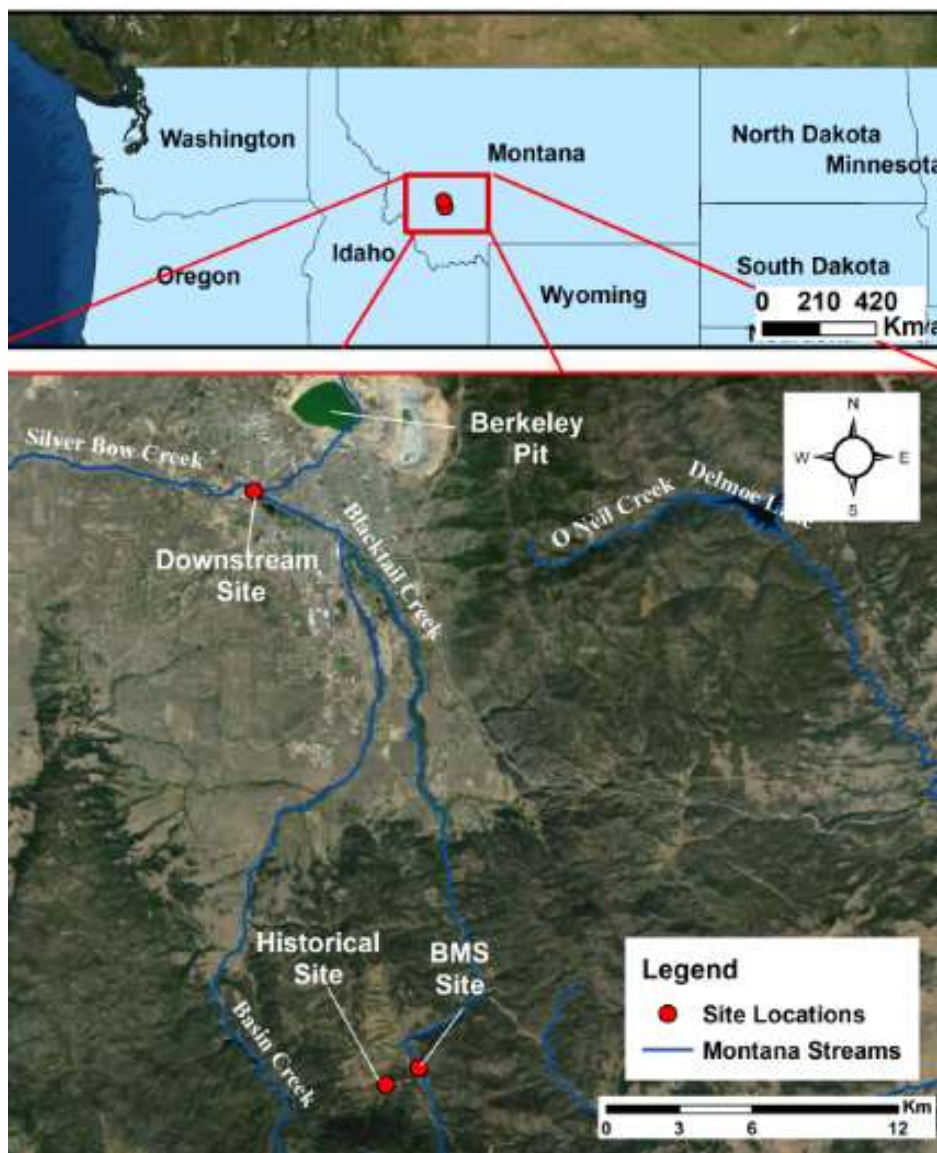


Figure 1: Location map of Butte, MT, and the study sites

The three sites are the primary focus of this project for pore water chemistry; however, ten surface water samples were collected along the stream to connect the sites spatially. In the three primary sites, sediment pore water samplers (peepers) were used to obtain high resolution chemistry of pore water spaces. Peepers are devices designed to sample sediment pore water and provide high vertical resolution chemistry profiles in sediment. Peepers contain 28 rows of cells evenly spaced 1 cm apart and deployed in sets of two. The cells are pre-filled with deionized

water and placed vertically in the sediment for two to three weeks. The cells then assimilate to the pore water chemistry and can be sampled efficiently.

1.2. Previous Studies

Previous work between the BMS and historical sites (upstream sites) and the valley superfund site (downstream site) have focused on different aspects. In the upstream restoration sites, previous work relates to the effectiveness of BMS, primarily how groundwater and the flood plain have been affected by the deployment of BMS, with comparisons along control reaches that have not been restored. In the upstream site, beavers are no longer present in the area, which resulted in breached beaver dams, stream incision, and a disconnect from the natural floodplain, and high sediment loads (Norman, 2020). Beaver dam mimicry structures were placed in the stream attempting to mimic natural beaver dams. The data since the erection of the structures have shown promising results in reconnecting the stream to its historically natural floodplain in this area and other regions (Pollock *et al.*, 2014; Norman, 2020). The BMS structures have slowed the surface flow of the creek to a point where suspended sediment is being deposited in the BMS area again. New sediment deposition is thought to have begun in October 2016 when the first structures were first put in place. Figure 2 is an example of an artificial beaver dam (BMS).



Figure 2: Example of a beaver mimicry structure in the BMS site

Sub-alpine streams, such as Blacktail Creek, are often narrow at the stream's higher elevations, and wider in the lower elevations (Wegener *et al.*, 2017). This tends to expel DIC through turbulence. Beavers tend to build their dams in the valleys where water is retained in alluvial sediments. Along with water, solutes are also retained within the alluvial sediments, especially fine grained glacio-fluvial sediments (Wegener *et al.*, 2017). These solutes often adsorb to fine grain sediments. While beaver dam areas retain water and solutes, they can either be sources or sinks depending on groundwater interactions. During high flow, the beaver dams act as sinks where water and other solutes become entrained in the floodplain. During baseflow, the dammed areas act as sources where water and solutes are released (Wegener *et al.*, 2017).

Peeper 20 and 21 were placed in the new stream bed sediment that appears to have been mostly deposited after BMS restoration. The peeper was placed in this location to gain an understanding of how new sediment can affect pore water chemistry. Figure 3 shows where the peeper was placed in the new sediments.

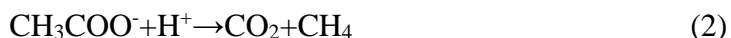


Figure 3: Peepers in the young sediment in the restoration site (left) sediment core take next to deployed peepers (right)

The historical site has a natural beaver dam that was constructed before the beavers were driven out of the region in a swamp with very still water. Sediments in this site are much finer because of the low velocity where this pond exists. The historical site is on the south fork of Blacktail Creek where the confluence is located downstream of both sites. The sediments are stained red which is likely due to iron oxide precipitation. Iron seeps are very common in the Butte Highlands, including in Basin Creek which flows adjacent to Blacktail.

The historical site is primarily a wetland with very slow rates of almost ponded flow. Wetlands in general contribute about 30% of the global methane production, making them the

largest natural source of atmospheric methane (Houghton et al., 2001; Bridgham et al., 2013; Comyn-Platt, 2018). Methane in the atmosphere retains about 84 times as much heat than CO₂, making it extremely potent as a greenhouse gas (Whiticar, 1999). Methane is produced under anoxic conditions and usually by the aid of methanogenic archaea. The most common form of methanogenesis is called acetoclastic methanogenesis, which is the process of breaking the acetate ion apart and facilitating electrons for energy in the absence of oxygen. Acetoclastic methanogenesis converts acetate to CH₄ and CO₂ by the reaction in Equation (2) (Whiticar, 1999; Gammons *et al.*, 2014; Parker *et al.*, 2016):



As seen in Equation 2, this process does not require the presence of oxygen, which makes it an anaerobic metabolic pathway. Acetate is formed during the breakdown of organic carbon under anoxic conditions. When methanogens breakdown the acetate ion, the resulting CO₂ is enriched in ¹³C and the conjugate CH₄ is depleted (Whiticar, 1999). This process has been observed near Butte in the sediments of Georgetown Lake (Shaw *et al.*, 2013; Gammons *et al.*, 2014; Parker *et al.*, 2016).

Figure 4 shows the deployment of peepers in the historical site. This site has much more vegetation and therefore more biogenic processes that could affect measurements such as dissolved oxygen, pH, and δ¹³C fractionations.



Figure 4: Peepers in older sediment in the historical site

Previous BMS studies have focuses on how nutrients and inorganic carbon behave compared to natural beaver dams. When beavers are present in an aquatic stream environment, the dams they construct influence sediment loading and analyte release. Using mass balance equations, Wegener *et al.* (2017) determined that nutrients are stored during snow melt and released during baseflow (Wegener *et al.*, 2017). Other studies have found similar results in both natural and artificial beaver dams (Westbrook *et al.*, 2013; Puttock *et al.*, 2017; Wegener *et al.*, 2017). Natural beaver dams have considerably more nutrients (NO_3^- , PO_4^{3-} etc.) associated with them. In contrast, wetland areas promote the decay of organic molecules, which promotes an anoxic environment. (Whiticar, 1999; Bridgham *et al.*, 2013).

In the downstream site, studies have used peepers to show reliable trends within the sediment pore water spaces for trace metals and nutrients. (Rader, 2019). There are very few

studies where peepers have been used to correlate DIC with trace elements; however, peepers have been used in Blacktail Creek in one previous study (Rader, 2019). Figure 5 shows the location of the peepers in the creek in the downstream site. Biogenic processes, such as sulfate reduction, have been documented in this site (Rader 2019; Robertson, 2019). The downstream site is located less than 1km downstream from the Diggings East and Northside tailings.



Figure 5: Downstream peeper 18 site in the Butte superfund site

Other previous studies in the downstream site have primarily focused on metal loading and the identification of different sources and sinks (Benner *et al.*, 1995; Balistrieri *et al.*, 2012, Rader, 2019).

Benner *et al.* (1995) found that the hyporheic zone can be both a source and a sink of metals Silver Bow Creek, depending on high flow or base flow. Hill and Duval (2009) and Devito and Dillon (1993) found that a beaver pond in Ontario, Canada retained nutrients during baseflow, and they were flushed during snowmelt. Several Montana Bureau of Mines (MBMG) open file reports have identified and discussed different sources and sinks of metal and nutrient contamination in Blacktail and Silver Bow Creeks (Metesh and Madison, 2004; Tucci, 2012; Tucci, 2014).

1.3. Scope of project

The goal of this project is to compare sediment pore water chemistry at the upland restoration site set in the mountains to the pore water chemistry lower in the valley Superfund site. I accomplish this by installing sediment pore water samplers (peepers) in these sites and by comparing surface water quality spatially along Blacktail Creek between the two primary sites. However, the upper highland sites consist of both newly deposited sediment from BMS restoration and pond sediments that have been accumulating for years or decades. Samples have been collected for water quality (temp, SC, DO, pH), metals, alkalinity, dissolved inorganic carbon (DIC), inorganic carbon isotope ratios ($^{13}\text{C}/^{12}\text{C}$), and nutrients (PO_4^{3-} , NO_3^- etc.). Photosynthesis, respiration and/or atmospheric equilibrium control much of the carbon cycling, which also influences trace elements (Gammons *et al.*, 2008; Gammons *et al.*, 2014).

Dissolved inorganic carbon (DIC) is one of the many analytes that peepers can be used to sample. In conjunction with DIC, $\delta^{13}\text{C}$ isotopes can demonstrate how isotopic fractionation takes place within the carbonate equilibrium system under different conditions (Karolyte *et al.*, 2017). Very few studies have used peepers to gather $\delta^{13}\text{C}$ gradients in DIC in stream sediment. Most DIC and $\delta^{13}\text{C}$ will be related to microbial interactions. When bicarbonate ($\text{HCO}_3^-_{(\text{aq})}$) is released by organisms, they leave an isotopically enriched bicarbonate due to preferred uptake of the depleted organic carbon. These factors can shift isotopic equilibrium which can be modeled in a similar way to systematic equilibrium.

1.4. Hypothesis and research questions

This project will attempt to categorize different sections of Blacktail Creek with respect to microbial processes and their effects on the geochemistry of Blacktail Creek. I expect to find evidence of hydrogeochemical processes that are associated with sub-alpine streams, mine related processes, and wetlands. The BMS site should primarily see aerobic respiration; the downstream site should see Mn and Fe oxide reduction and sulfate reduction; and the historical site should see primarily methanogenesis. The BMS site should be mostly aerobic due to the coarser grained nature of the sediments upstream. The downstream site sediments are related to mining processes which usually see Mn and Fe, oxide reduction, and sulfate reduction.

2. Methodology

2.1. Field Methods

Field samples were collected directly from the stream or with a peristaltic groundwater pump by Geotech Environmental Equipment, Inc. and pumped directly in containers properly prepared and stored based on analyte specific recommendations. Groundwater wells were purged and allowed to recharge into the well to collect and maintain accurate and representative data. In November, ground water levels were low and partially frozen which made it difficult to measure specific conductivity, pH, or collect other analytes so only DIC and $\delta^{18}\text{O}/\delta\text{D}$ were collected. These data were primarily used to track sources of surface water in the creek. Sediment pore water samplers (peepers) were also used to collect samples. Analytes include DIC, $\delta^{18}\text{O}/\delta\text{D}$, major cations, major anions, trace elements, alkalinity, sulfide, and phosphate.

Peepers, as described by Hesslein (1976) were used to gather high resolution chemistry in the shallow subsurface of Blacktail Creek. The peepers in this study were purchased from Rickly Hydrological Co., Inc. Peepers with 10-ml cells or 5-ml cells were combined to produce a total of 28 cm of sediment pore water chemistry profile. Figure 6 shows the size and dimensions of the peepers as well as how pore water diffusion is thought to take place.

Peepers are made of two pieces of plastic with a nylon membrane in between. The main piece has 5- and 10-mL cutouts that are filled with deionized water and alternate 1 cm apart. A piece of nylon membrane sits on top of the main piece with cut outs. The nylon membrane has pore spaces that are approximately .5 microns wide allowing for effective diffusion to take place across the nylon membrane and equilibrate with the pore water spaces while keeping most of the sediment out. The second piece of plastic is on top of the nylon and main plastic and is screwed

on tightly to prevent cross contamination between cells. Figure 6 shows a diagram of how peepers behave in the sub surface and how they are assembled.

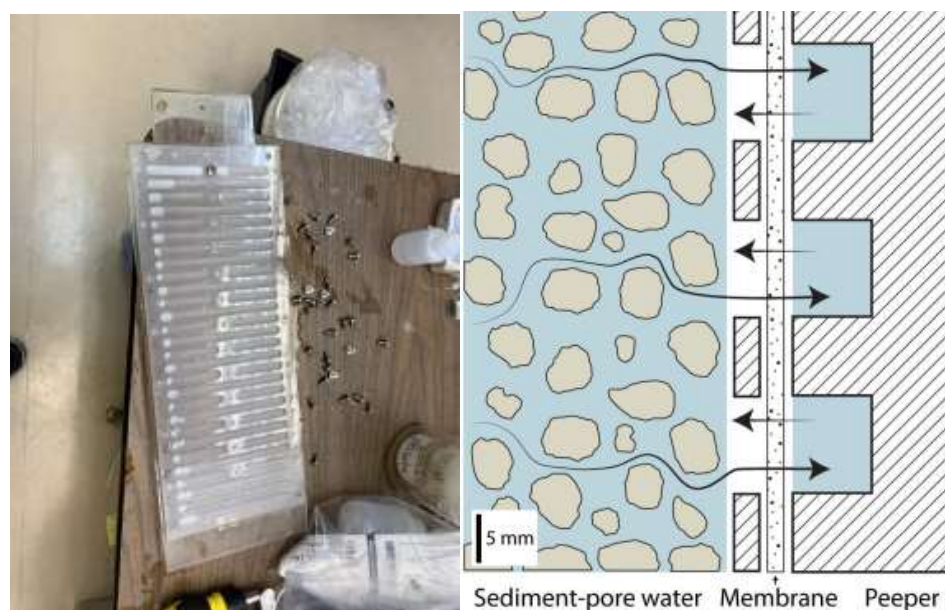


Figure 6: Peeper setup, left is peeper sets, right (Rader, 2019) is schematic of a peeper in the sediment column

2.2. Peeper preparation, deployment, and sampling

Preparing for sediment pore water sampling included filling each peeper cell with N_2 or Ar purged deionized water. Pre-weighed and pre-diluted containers appropriate for each analyte were prepared in conjunction with each peeper. The peepers were stored in deionized water that had been purged with argon or nitrogen to keep the cells anoxic until sample collection.

Two peepers were placed side by side, about 6 inches apart, in the stream bed. The top four cells of the peepers were not below the sediment water interface (they were exposed above the sediment directly in the water column). A sediment core was collected to help correlate trends with finer and coarser grained sediments. The peepers were left in the stream bed for a

minimum of three weeks and then sampled. During sampling, a glove bag was filled with argon gas, to keep conditions anoxic during sampling, and the peepers were placed inside the glove bag. A 60 mL syringe equipped with a syringe needle is used to penetrate the glove bag and nylon membrane. The sample aliquot is then drawn into the 60 mL syringe. After the needle is removed, a 0.2-micron syringe filter is placed onto the end of the syringe and the contents of each cell were placed in the pre-weighed containers and properly labeled. All sample bottles were pre-loaded with deionized water for dilution and pre-massed. After sampling, sample bottles were weighed with deionized water and sample that allowed for precise dilution factors.

Downstream peepers were collected and analyzed for metals, alkalinity, and ions but not used until this study. These samples were collected independently from this study. DIC samples were collected but not analyzed until this project. The DIC samples were collected on October 2nd and analyzed in early January. Prior to analysis, samples were stored at 4°C. Table I shows the general layout of each analyte that the cells were sampled for.

Table I: General peeper layout of each of the three sets of peepers

Cell	ICP-MS/OES	IC	Alkalinity	DIC	PO ₄ ³⁻ or H ₂ S
Surface (no dilution)					
1 (5 ml cells)					
2 (10 mL cell)					
3 (5 ml cells)					
4 (10 mL cell)					
5 (5 ml cells)					
6 (10 mL cell)					
7 (5 ml cells)					
8 (10 mL cell)					
9 (5 ml cells)					
10 (10 mL cell)					
11 (5 ml cells)					
12 (10 mL cell)					
13 (5 ml cells)					
14 (10 mL cell)					
15 (5 ml cells)					
16 (10 mL cell)					
17 (5 ml cells)					
18 (10 mL cell)					
19 (5 ml cells)					
20 (10 mL cell)					
21 (5 ml cells)					
22 (10 mL cell)					
23 (5 ml cells)					
24 (10 mL cell)					
25 (5 ml cells)					
26 (10 mL cell)					
27 (5 ml cells)					
28 (10 mL cell)					

Alkalinity was measured and reported as ppm of CaCO₃ using a Hach digital titrator, loaded with 0.16N H₂SO₄ and bromocresol red indicator packets (HACH method 8203). Peeper cells containing approximately 10 mL of sample water were extracted and added to 40 mL of deionized water. These aliquots were not filtered. The reading on the digital titrator must be

corrected for dilution since this Hach method calls for 100 mL of sample and the peepers only have a max volume of 10 mL. Equation(3) was used to correct for dilution:

$$\text{corrected alkalinity} = \frac{(\text{raw value} \times 100)}{\text{sample mass}} \quad (3)$$

where sample mass is the pre-collection mass subtracted from the post collection mass in grams. The raw value is the number of “clicks” on the digital titrator which dispenses the amount of H₂SO₄ required for the sample to reach the endpoint before correcting for dilution. This equation requires the use of 0.1600N H₂SO₄ cartridge.

Surface water and groundwater samples were not diluted. For surface water, 50 mL of water was measured in a volumetric flask and then transferred to a 120 mL Erlenmeyer flask. Bromocresol red indicator was added and the same 0.16N H₂SO₄ titrant was added until the end point.

2.3. Analytical Methods

For measurements that cannot be taken directly in the field, appropriate sample collection is necessary. Most analytical work was done at the MBMG.

2.3.1. Dissolved inorganic carbon (DIC)

Prior to sampling, all 40 mL glass vials were “muffled” (heated) in a furnace for 4 hours at 400°C to convert any residual carbon into CO₂ gas. DIC vials were prepared by adding 30 mL of deionized water to each glass vial appropriate for carbon analysis. During sampling, 10 mL of filtered sample were added to the pre-diluted vials using the 60ml syringe. Dissolved inorganic carbon and dissolved organic carbon were analyzed using a Picarro cavity ringdown spectrometer (CRDS) and Aurora Total carbon analyzer. Samples are placed in the Aurora and

reacted with 5% v/v phosphoric acid. The calibration curve was made with 5 standards each of Li_2CO_3 and NaHCO_3 . Standards ranged from 0 mg C L^{-1} to 50 mg C L^{-1} . Samples are run in triplicate and uncertainty is gauged using the standard deviation of each sample. Standard deviation is usually 0.5 mg C L^{-1} (or lower) but can vary depending on contamination and other factors. To ensure cross contamination due to carryover does not occur between each sample, 5% v/v phosphoric acid vials, followed by deionized water blanks, were placed in between each surface water sample. Peeper samples were diluted enough where cross contamination was not an issue. The concentration of DIC in the sample is then corrected for dilution using the pre-determined dilution factor described above. The amount of CO_2 is measured and is then transferred to the Picarro which can then detect isotopic ratio of $^{13}\text{C}/^{12}\text{C}$ using cavity ringdown spectrometry (CRDS). Li_2CO_3 has standard isotopic composition of -6.38‰ and NaHCO_3 has an isotopic composition of -23.05‰. These values are then used to create a standard curve to determine the isotopic composition compared to VPDB.

2.3.2. ICP-MS and ICP-OES

Sample vials were prepared by adding 20 mL of deionized water and 0.3mL of 10% HNO_3 to 60 mL HDPE bottles that had been acid washed for a minimum of 2 days in concentrated HNO_3 . Samples were taken to the MBMG Analytical Lab for analysis. Trace elements (Cu, Zn, Mn, Fe, and Pb) were determined by EPA method 200.8 using a Thermo Scientific iCAP Q ICP-MS.

ICP-OES (also at the MBMG) was analyzed from the same bottles as ICP-MS. The MBMG uses a Thermo Scientific iCAP 6000 Series ICP-OES following EPA Method 200.7. This method is more appropriate for major cations K^+ , Na^+ , Ca^{2+} , Mg^{2+} , Fe^{2+} , Mn^{2+} . Method 200.7 measures total elements and does not speciate between different ions like Fe^{2+} and Fe^{3+} .

Geochemical modeling or spectroscopy would be required to determine the percentage of each ion.

2.3.3. Ion Chromatography

Sample vials were prepared by adding 20 mL of deionized water to HDPE bottles that were pre-weighed to correct for dilution. Major anions (Cl^- , F^- , NO_2^- , NO_3^- , PO_4^{3-} , SO_4^{2-}) were measured with a Metrohm Compact IC Plus (EPA Method 300.1). Samples were corrected for dilution after analysis by multiplying the raw number by the pre-determined dilution factor.

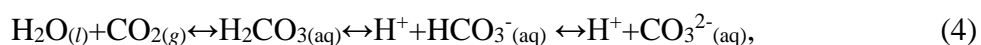
2.4. Sediment cores

A sediment core was taken next to each set of peepers. The cores were used to correlate the fine grain sediments with higher analyte concentration in the peepers. Analysis was purely visual and only an estimate of grain size, no sieve analysis was performed.

2.5. Equations and Calculations

2.5.1. Estimating pH

By using Equation (4):



it is possible to estimate the pH within the peeper cells. Estimated pH can be used to gather information on speciation of metals and ions. Since carbonic acid is a diprotic acid, there are two acid dissociation equilibrium constants known as pKa values, pKa₁ and pKa₂. We ignored pKa₂ and CO_3^{2-} because there is usually an insignificant amount of CO_3^{2-} in natural streams and waters. Concentrations of CO_3^{2-} are usually around 10^{-7} ppm, which is insignificant compared to 10^{-3} and 10^{-4} for CO_2 and HCO_3^- and can be ignored for calculations. Figure 7 (left) shows the $\log f\text{O}_2$ vs pH diagram of the carbonate system. Given that the Hydrolab measured pH values in

the surface water were within the 6 to 8 range, we can safely assume that there is a negligible amount of CO_3^{2-} and the dominant species in the creek water is HCO_3^- . Figure 7 shows the relative proportions of each DIC species at different pH and redox conditions.

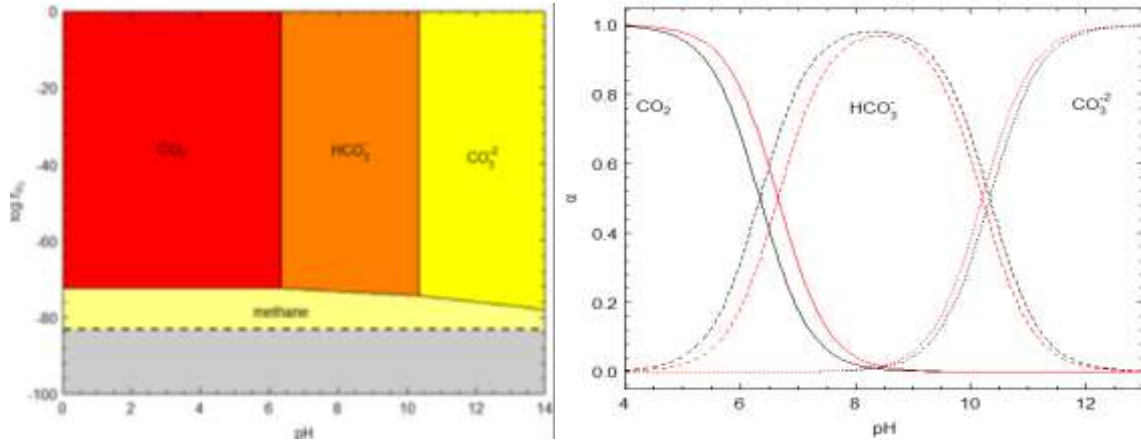


Figure 7: log $f\text{O}_2$ vs pH (left) and Bjerrum plot of inorganic carbon (right) where α is activity of inorganic carbon divided by mole fraction of DIC (Dick, 2019)

DIC measures all inorganic carbon in the system, so this can be divided into each of its constituents with Equation (5):

$$\text{DIC} = \text{H}_2\text{CO}_3 + \text{HCO}_3^- + \text{CO}_3^{2-} \quad (5)$$

where DIC is total unfiltered inorganic carbon (mg C L^{-1}) measured in the creek or peeper cell. We assume that $\text{HCO}_3^-(\text{aq})$ makes up most of the alkalinity in the system, so it is acceptable to use values from the alkalinity data in Equation 3. Values of alkalinity were converted from $\text{mg L}^{-1} \text{CaCO}_3$ to $\text{mg L}^{-1} \text{HCO}_3^-(\text{aq})$. As previously mentioned, we assume that $\text{CO}_3^{2-}(\text{aq})$ is negligible compared to the amount of $\text{H}_2\text{CO}_3(\text{aq})$ and $\text{HCO}_3^-(\text{aq})$. Other sources of alkalinity may exist in the surface water and sediment. DIC is the measure of dissolved $\text{CO}_2(\text{aq})$ and $\text{HCO}_3^-(\text{aq})$. Subtracting DIC from $\text{HCO}_3^-(\text{aq})$ gives the amount of dissolved $\text{CO}_2(\text{aq})$ in the creek as $\text{H}_2\text{CO}_3(\text{aq})$.

Since the pH in the top peeper cell was always exposed to roughly the lower middle part of the water column, it can be compared with pH measured with a Hydro lab reported value. The pH of the entire aquatic system can be influenced by microbes, metal complexes and hydration rings around $\text{H}_3\text{O}^+_{(aq)}$.

2.5.2. Calculating flux for metals and DIC

Diffusive flux was calculated for iron, manganese, arsenic, and DIC. Diffusive flux is heavily influenced by whether the chemical species is considered conservative or not. Arsenic and manganese are generally considered conservative in the species arsenate (AsO_4^{3-}) and Mn^{2+} , respectively. This is done by using Fick's first law as shown in Equation (6):

$$J = \phi D_s \frac{dC}{dz} \quad (6)$$

where J is the specific diffusive flux of solute ($\mu\text{g cm}^{-2} \text{d}^{-1}$); ϕ is the sediment porosity (unitless) and was estimated to be 0.3 for average stream bed sediments (Fetter, 2001; Rader, 2019); D_s is the diffusion coefficient ($\text{cm}^2 \text{sec}^{-1}$); dC is the dissolved metal concentration ($\mu\text{g L}^{-1}$) difference between cells 4 and 14, and dz is depth below the sediment water interface (SWI) measured in cm. Porosity can vary slightly between sites. Fine sands and clays can range between 0.2 and 0.5. Any porosity within this range is minor, however a large increase in porosity increases flux by about one order of magnitude. Porosity matters less, when there is a higher concentration gradient.

Flux is driven by concentration gradient from high concentration to low concentration.

The concentration gradient in the sediment column was also calculated using Equation (7):

$$\frac{dC}{dz} = \frac{C_{sw} - C_{pw}}{\Delta z} \quad (7)$$

where C_{pw} is the pore water concentration at a depth of 10 cm in the sediment, C_{sw} is the concentration in the water column, and Δz is the difference in depth (10 cm). Positive values of dC indicate flux into the stream and negative values indicate flux into the sediment.

D_s was calculated with the following D_0 constants for their respective analyte in Table II. The equation for calculating D_s is shown in Equation (8):

$$D_s = \phi^2 D_0 \quad (8)$$

Table II shows the D_0 constants were taken from Li and Gregory, 1974 and Tanaka *et al*, 2013:

Table II: Diffusive flux constants where units of D_0 are ($\mu\text{g sec}^{-1} \text{cm}^{-2}$)

Analyte	Species	D_0 0°C	D_0 18°C	D_0 25°C	Source
As	H_2AsO_4^-			9.05×10^{-6}	Tanaka, 2013
Fe	Fe^{2+}	3.41×10^{-6}	5.82×10^{-6}	7.19×10^{-6}	Li and Gregory, 1974
Fe	Fe^{3+}		5.28×10^{-6}	6.07×10^{-6}	Li and Gregory, 1974
Mn	Mn^{2+}	3.05×10^{-6}	5.75×10^{-6}	6.88×10^{-6}	Li and Gregory, 1974
C	CO_2		16.0×10^{-6}		Li and Gregory, 1974

Dispersivity (D_s) values were calculated using the value that represents the thermodynamic parameters most closely.

2.5.3. Partitioning inorganic carbon isotopes between H_2CO_3 and HCO_3^-

When DIC is analyzed, bulk concentration of carbon is determined as well as the bulk isotopic composition of carbon ($\delta^{13}\text{C}_{\text{DIC}}$). The bulk isotopic composition of DIC can be partitioned into its constituent components based on Equation (9) from

(Zhang *et al* 1995; Clark and Fritz, 1997; Young, 2002; Zhang *et al*, 2015; Lehn *et al*, 2017):

$$\delta^{13}\text{C}_{\text{DIC}} = \delta^{13}\text{C}_{\text{H}_2\text{CO}_3} \cdot \text{XH}_2\text{CO}_3 + \delta^{13}\text{C}_{\text{HCO}_3^-} \cdot \text{XHCO}_3^- + \delta^{13}\text{C}_{\text{CO}_3^{2-}} \cdot \text{XCO}_3^{2-} \quad (9)$$

where $\delta^{13}\text{C}_{\text{DIC}}$ is the bulk isotopic composition obtained from the Picarro, $\delta^{13}\text{C}_{\text{H}_2\text{CO}_3}$ is the isotopic composition of carbonic acid, $\delta^{13}\text{C}_{\text{HCO}_3^-}$ is the isotopic composition of bicarbonate, $\delta^{13}\text{C}_{\text{CO}_3^{2-}}$ is the isotopic composition of carbonate, XH_2CO_3 is the mole fraction of carbonic acid,

$X\text{HCO}_3^-$ is the mole fraction of bicarbonate and $X\text{CO}_3^{2-}$ is the mole fraction of carbonate. As mentioned previously, $\delta^{13}\text{C}_{\text{CO}_3^{2-}}$ can be ignored because it is insignificant compared to $\delta^{13}\text{C}_{\text{H}_2\text{CO}_3}$ and $\delta^{13}\text{C}_{\text{HCO}_3^-}$. Ignoring carbonate yields Equation (10):

$$\delta^{13}\text{C}_{\text{DIC}} = \delta^{13}\text{C}_{\text{H}_2\text{CO}_3} X\text{H}_2\text{CO}_3 + \delta^{13}\text{C}_{\text{HCO}_3^-} X\text{HCO}_3^- \quad (10)$$

where factors are the same as above. Another related equation is required in order to determine both unknowns in Equation 10. Using isotopic equilibrium Equation (1):

$$\delta^{13}\text{C}_{\text{HCO}_3^-} = \delta^{13}\text{C}_{\text{H}_2\text{CO}_3} + 9.5\text{‰} \quad (11)$$

where 9.5‰ is a constant based on temperature determined from a table of inorganic carbon isotopic equilibrium constants based on temperature (Clark and Fritz, 1997). Equation 12 is based on the following equation 13

$$1000 \ln \alpha_{\text{HCO}_3^- \text{H}_2\text{CO}_3} = \delta^{13}\text{C}_{\text{HCO}_3^-} - \delta^{13}\text{C}_{\text{H}_2\text{CO}_3} \quad (12)$$

where α is the isotopic differential constant determined from Clark and Fritz (1997) based on temperature. A temperature of 4°C is most representative of all three peeper sets and has a $\Delta\text{HCO}_3^- \text{H}_2\text{CO}_3$ of 9.5‰ (Clark and Fritz, 1997). Using this relationship, Equation (11) is derived by substituting $\delta^{13}\text{C}_{\text{HCO}_3^-}$ for $\delta^{13}\text{C}_{\text{H}_2\text{CO}_3} + 9.5\text{‰}$:

$$\delta^{13}\text{C}_{\text{DIC}} = \delta^{13}\text{C}_{\text{H}_2\text{CO}_3} f_{\text{H}_2\text{CO}_3} + (\delta^{13}\text{C}_{\text{H}_2\text{CO}_3} + 9.5\text{‰}) f_{\text{HCO}_3^-} \quad (11)$$

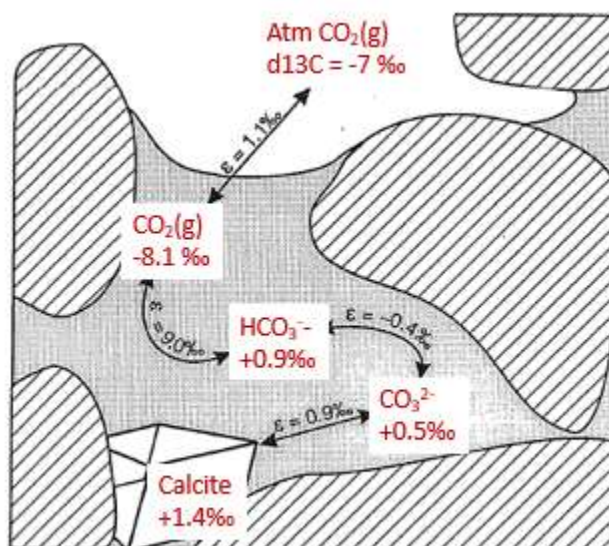


Figure 8: Diagram from (Clark and Fritz, 1997) showing isotopic equilibrium exchange during speciation transfer of carbon

Figure 8 visually showing how to account for the isotopic mass balance in the sediment pore water spaces. The values used in the diagram are adjusted for stream conditions at 1 bar pressure and 4° C. For warmer stream conditions, a chart is used to correct for isotopic exchange. This project used Clark and Fritz (1996).

3. Results

The following text refers to the dilution-corrected data sets based on peepers, surface water, and ground water. Peeper data are plotted with depth above the SWI on the y-axis and analyte concentration/value on the x-axis. Measured surface water data are in table format and figures are in distance downstream on the x-axis and concentration or ratio on the y-axis. Sampling dates were recorded and placed in Table III. Sample sites can have different chemistry based on the day it was sampled. For example, if a precipitation event occurred before sampling, that can increase groundwater flow temporarily. This would mean that the chemistry is influenced more by groundwater.

Table III: Sampling dates for peepers, groundwater, and surface water

Sample Type	Date sampled
Peeper 18 and 19	October 2 nd 2019
Peeper 20 and 21	November 5 th 2019
BMS ground and surface water	November 11 th 2019
Peeper 22 and 23	August 27 th 2020
Blacktail Creek Surface	September 18 th 2020

3.1. Lower Blacktail Creek (Peepers 18 and 19)

Peepers 18 and 19 were placed in the lower Blacktail Creek remediation area within city limits of Butte, Montana, near the confluence of Silver Bow Creek. Figure 9 and Figure 10 show individual solute and analyte concentrations and values. At the time of peeper sampling, the surface water had a pH of 7.84, temperature of 9.14°C, SC of 300 $\mu\text{S}/\text{cm}$, and ORP of 345 mV.

Samples were collected and analyzed for metals and trace elements (using ICP-MS and ICP-OES), alkalinity, and anions (using IC), but were not reported until this project. DIC was also collected, but never analyzed until this project. Values for iron were combined from ICP-OES and ICP-MS; data was reported based on the instrument's detection limits. Values under 0.15mg L⁻¹ used ICP-MS results rather than ICP-OES. Peeper cells 0, 2, 4, and 6 were near or

below the detection limit. Data for peeper cells deeper than cell 6 were taken from the ICP-OES because the data obtained from ICP-MS values were over the linear range of the iron standards.

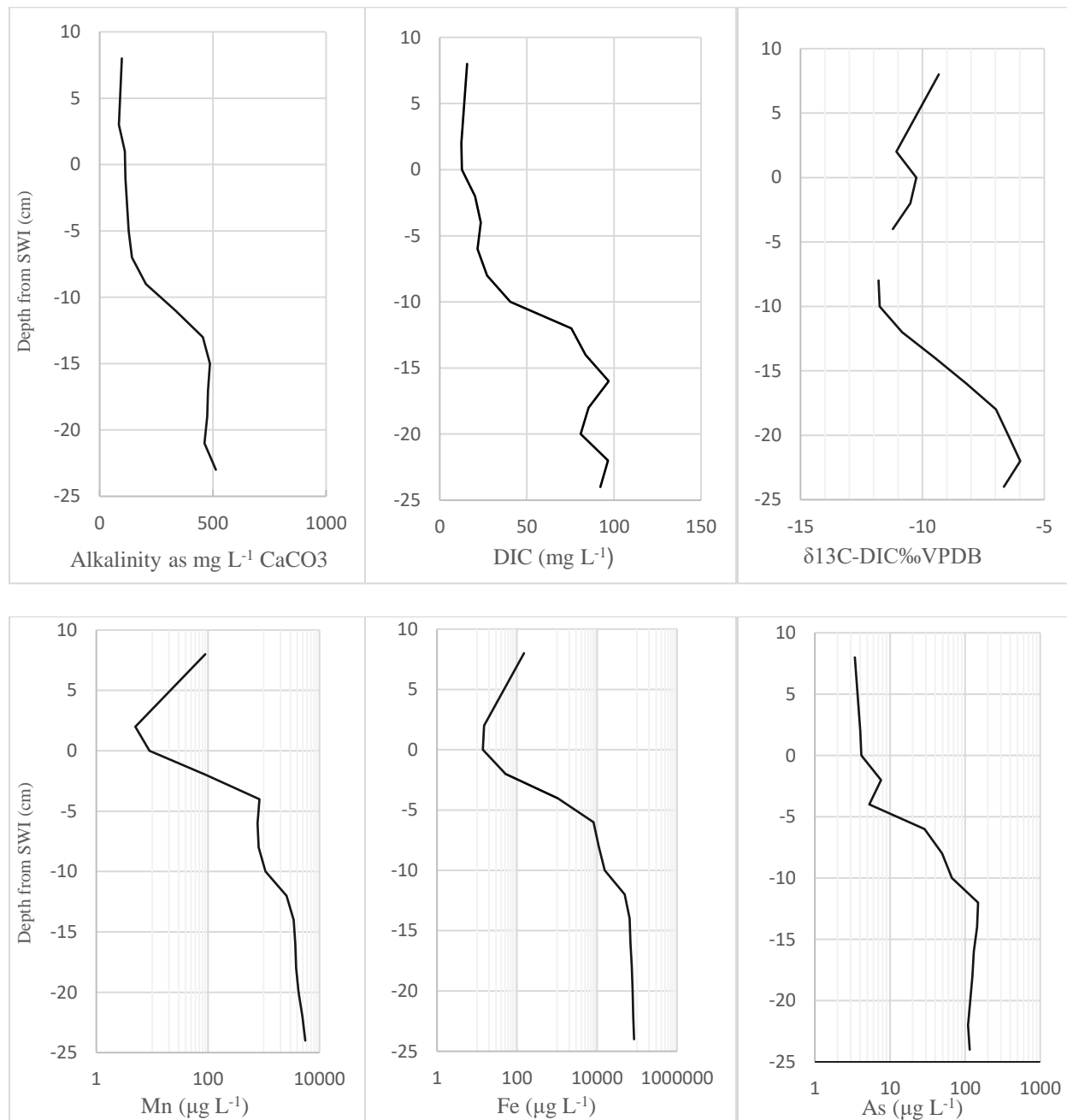


Figure 9: Peeper 18 results, 0 represents the sediment water interface (SWI). Note metals are on a log x axis and each graph has a different scale that shows its profile more clearly.

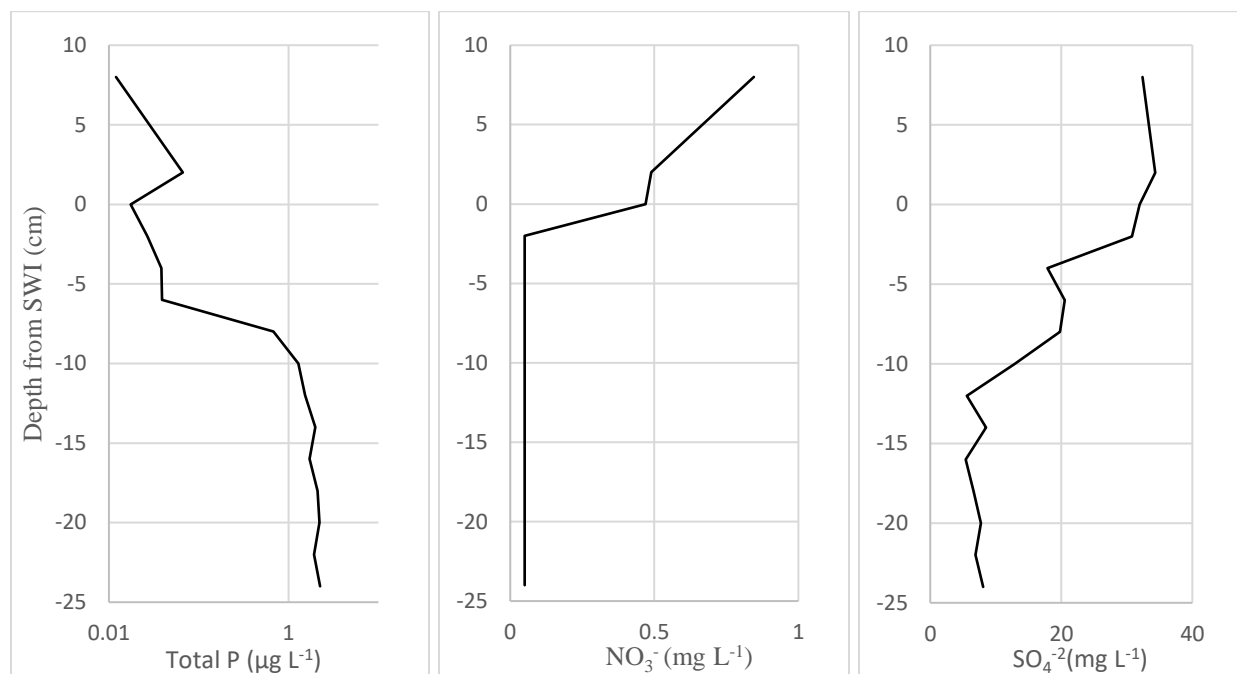


Figure 10: Peeper 18 downstream results for P, NO₃⁻, and SO₄²⁻, NO₃⁻ is below detection limit below 0cm

DIC samples were stored in 4°C and over time, the iron oxides that precipitated out in unacidified samples could be seen visually. Samples that were analyzed by ICP-MS and ICP-OES were preserved with 10% HNO₃ v/v, which helped keep iron dissolved. DIC was not preserved with acid (low pH would expel DIC) so a major concern was the potential for siderite to be precipitated among the iron oxides. Siderite is an iron carbonate mineral that can precipitate in low amounts under favorable conditions. The DIC concentrations would be inaccurate if siderite precipitated out of solution. Using the CHNOSZ geochemical modeling package in R to model the conditions, it is unlikely that a significant amount of siderite could have precipitated (Figure 11). Conditions were adjusted to match the *in-situ* conditions of the sample based on field measurements. Hematite (Fe₂O₃) or amorphous hydrous ferric oxide (HFO) is much more likely to be the observed precipitate in the unacidified samples. Phosphate was analyzed on the ion

chromatograph; samples were prepared without the addition of acid. This caused the phosphate to sorb to the precipitated iron oxides. Total phosphorous is likely in the form of phosphate.

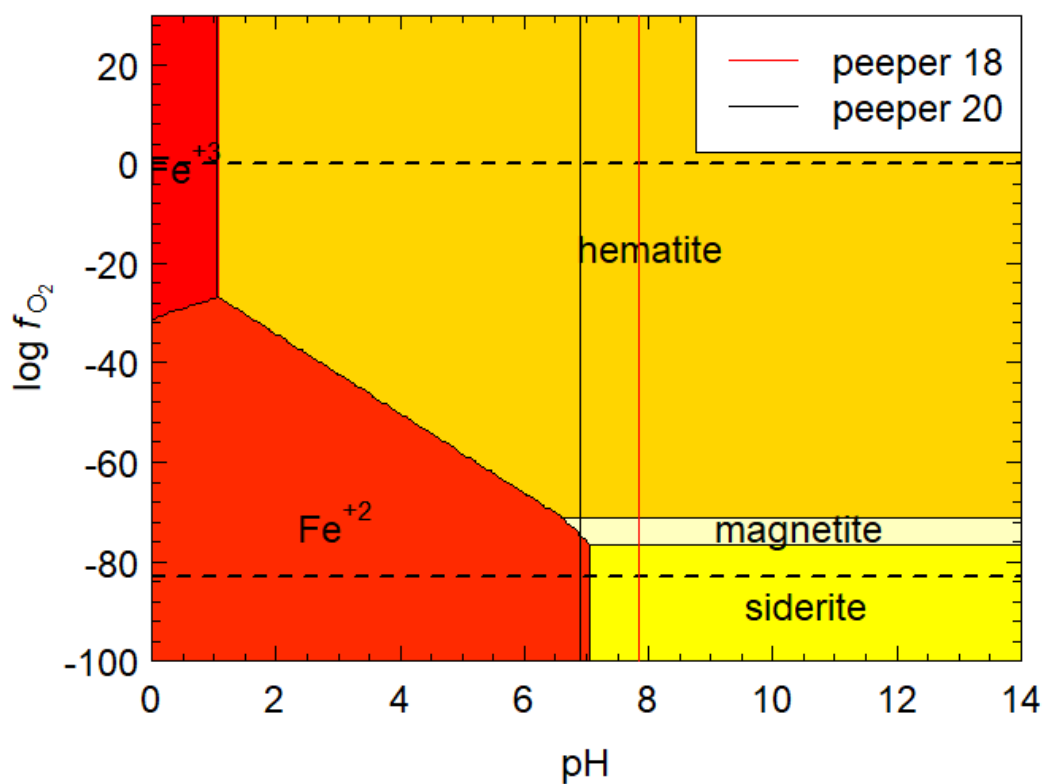


Figure 11: Iron speciation diagram, 1 bar pressure, 25° C, $CO_2 = 0.01$ (Dick, 2019)

Most metals appear to increase 10 to 50-fold in concentration in the sediment column compared to the surface water.

3.1.1. Speciating DIC

By taking the difference between total DIC and alkalinity as HCO_3^- it is possible to calculate the amount of dissolved CO_2 present in the aqueous phase in the sample. Figure 12 shows the difference between DIC and alkalinity in peepers 18 and 19.

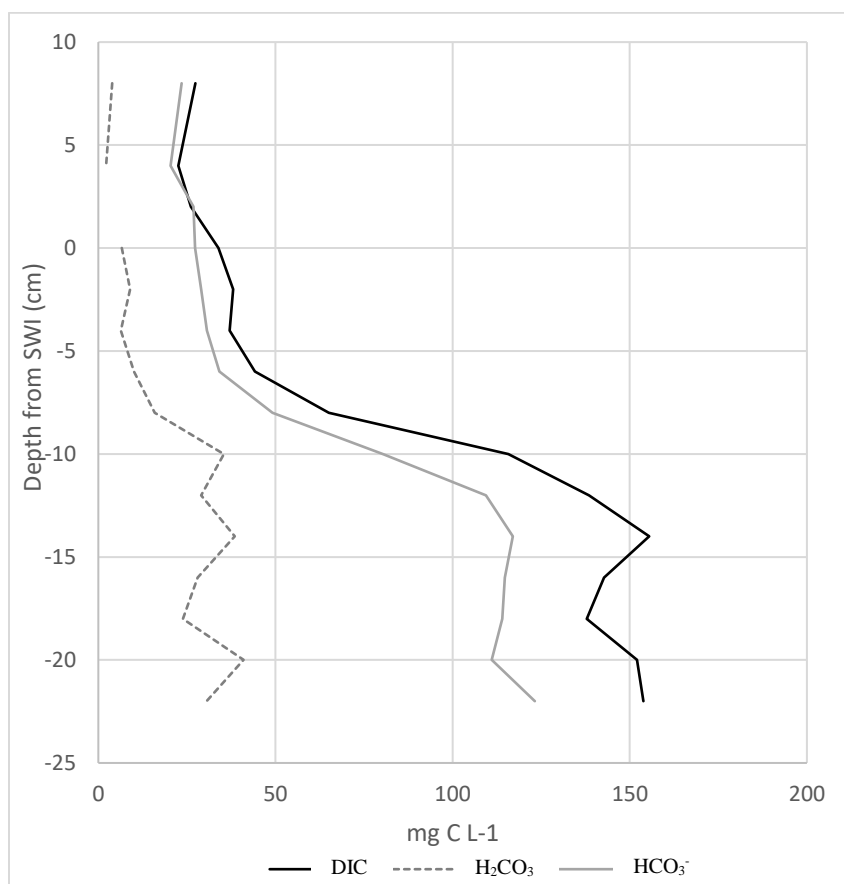


Figure 12: Difference between DIC and Alkalinity shows H₂CO₃

The metals appear to increase in concentration from 2 cm to 12 cm below SWI, while DIC and alkalinity both begin to increase in concentration at 10 cm below SWI.

3.1.2. DIC isotope partitions

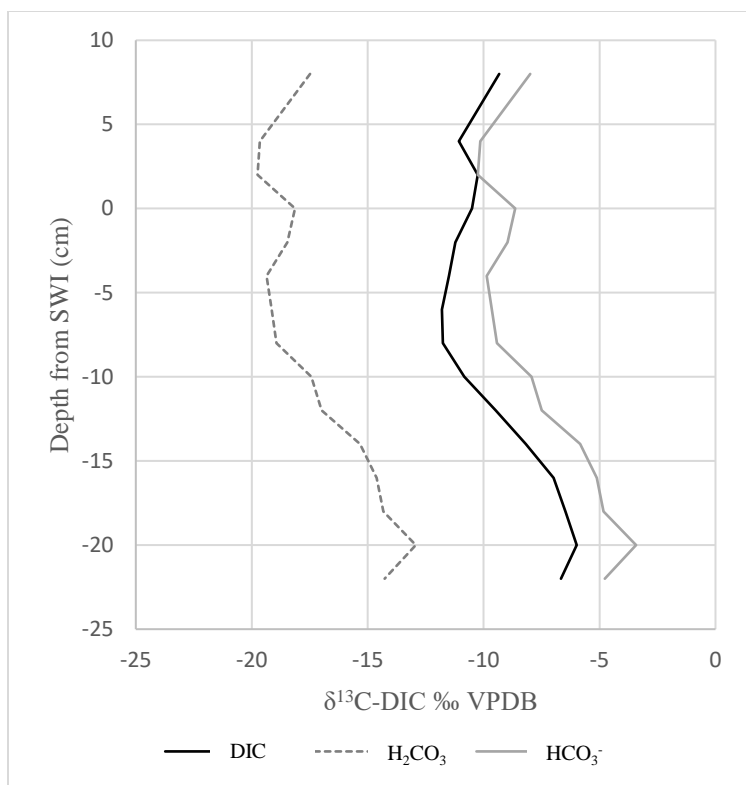


Figure 13: δ¹³C Isotope partitions in Peeper 18

Results of calculating $\delta^{13}\text{C}_{\text{H}_2\text{CO}_3}$ and $\delta^{13}\text{C}_{\text{HCO}_3^-}$ in Figure 13 show the relative proportions of $\delta^{13}\text{C}$ between carbonic acid and bicarbonate to total dissolved inorganic carbon.

3.1.3. Sediment core

No sediment core was taken at the downstream site, but fine to very fine grain sediment was noted at this site. Sediment grains include muscovite, biotite, pyrite, and quartz. The peeper data suggest finer grain silts or clays below 10cm. Higher analyte concentrations at depth can usually be attributed to adsorption of analytes onto pelitic minerals.

3.1.4. Estimated pH

The downstream peeper site had the highest percent error of the top peeper cell with the hydro lab measurement value. This is likely due to microbial processes. However, these values

can still be useful for modeling. Table IV shows the results for calculating pH using the carbonate equilibrium system. Using an acid equilibrium value (K_a) of 2.77971×10^{-7} , the carbonate equilibrium equation was rearranged to solve for activity of hydrogen ions and then converted to pH. A Hydrolab was used to measure the pH of surface water near the upper most peeper cells to compare the two methods of measuring and calculating pH. The Hydrolab gave a pH of 7.84. The calculated pH for the upper most peeper cell, using the carbon numbers, was 6.37. This disagreement could also be reflecting diel cycling which has been observed in the creek before (Gammons *et al.*, 2005).

Table IV: Calculated pH of peepers 18 and 19

Depth from SWI (cm)	DIC mg C L ⁻¹	Alkalinity as mg L ⁻¹ CaCO ₃	HCO ₃ ⁻ (mg C L ⁻¹)	H ₂ CO ₃ (mg C L ⁻¹)	calculated pH
Surface	27.4	98.1	23.5	3.87	7.08
2	6.49	85.0	20.4	2.19	7.27
0	6.96	112	26.8	error	error
-2	9.46	114	27.3	6.65	6.91
-4	10.6	121	29.1	9.01	6.81
-6	11.0	128	30.7	6.37	6.98
-8	12.6	142	34.2	10.0	6.83
-10	18.6	205	49.1	15.9	6.79
-12	32.7	335	80.3	35.4	6.66
-14	39.8	456	109	29.1	6.88
-16	43.1	487	117	38.5	6.78
-18	37.0	478	115	28.0	6.91
-20	38.9	475	114	23.9	6.98
-22	39.7	463	111	41.0	6.73
-24	41.8	513	123	30.6	6.90

3.1.4.1. Diffusive flux in the downstream site

The downstream site has the most metal flux from the sediment. This is also shown in Rader (2019). The higher concentration below the SWI suggests that there is an upward flux of Fe, Mn, and As into the stream. The diffusive flux was calculated using a constant depth of 10cm below the SWI and is shown in Table V. Porosity can vary in each peeper site; however, in each of the three peeper sites the sediment was fine to very fine at the -10 cm depth.

Table V: Diffusive flux in peeper 18 downstream site where D_o , D_s , and J are in units of $(\mu\text{g s}^{-1} \text{cm}^{-2})$

Analyte	Surface ($\mu\text{g L}^{-1}$)	Pore ($\mu\text{g L}^{-1}$)	dC ($\mu\text{g L}^{-1}$)	dC/dz ($\mu\text{g L}^{-1} \text{cm}^{-1}$)	Porosity	D_o	D_s	J
As	4.17	66.7	-65.5	6.25	0.30	9.05×10^{-6}	8.15×10^{-7}	1.53×10^{-6}
Fe	20.0	1.56×10^4	-1.56×10^4	1.56×10^3	0.30	5.28×10^{-6}	4.75×10^{-7}	2.22×10^{-4}
Mn	20.0	1.07×10^3	-1.05×10^3	105	0.30	5.75×10^{-6}	5.18×10^{-7}	1.63×10^{-5}
DIC	2.61×10^4	6.50×10^4	-3.89×10^4	3.89×10^3	0.30	1.60×10^{-5}	1.44×10^{-6}	1.68×10^{-3}

3.2. Upper Blacktail Recently Deposited Sediment (Peeper 20 and 21)

Peeper 20 and 21 were placed in the post BMS restoration sediments. Figure 14 and Figure 15 shows individual analyte concentrations and $\delta^{13}\text{C}$ isotope values. The surface water had a pH of 6.91, temperature of 2.00°C , SC of $176.6 \mu\text{S/cm}$, and ORP of -171 mV . Iron, manganese, and arsenic appear to follow similar trends at different concentrations. DIC and alkalinity were collected from different peeper cells but show identical trends. The $\delta^{13}\text{C}$ values becoming more depleted near the bottom of the peeper.

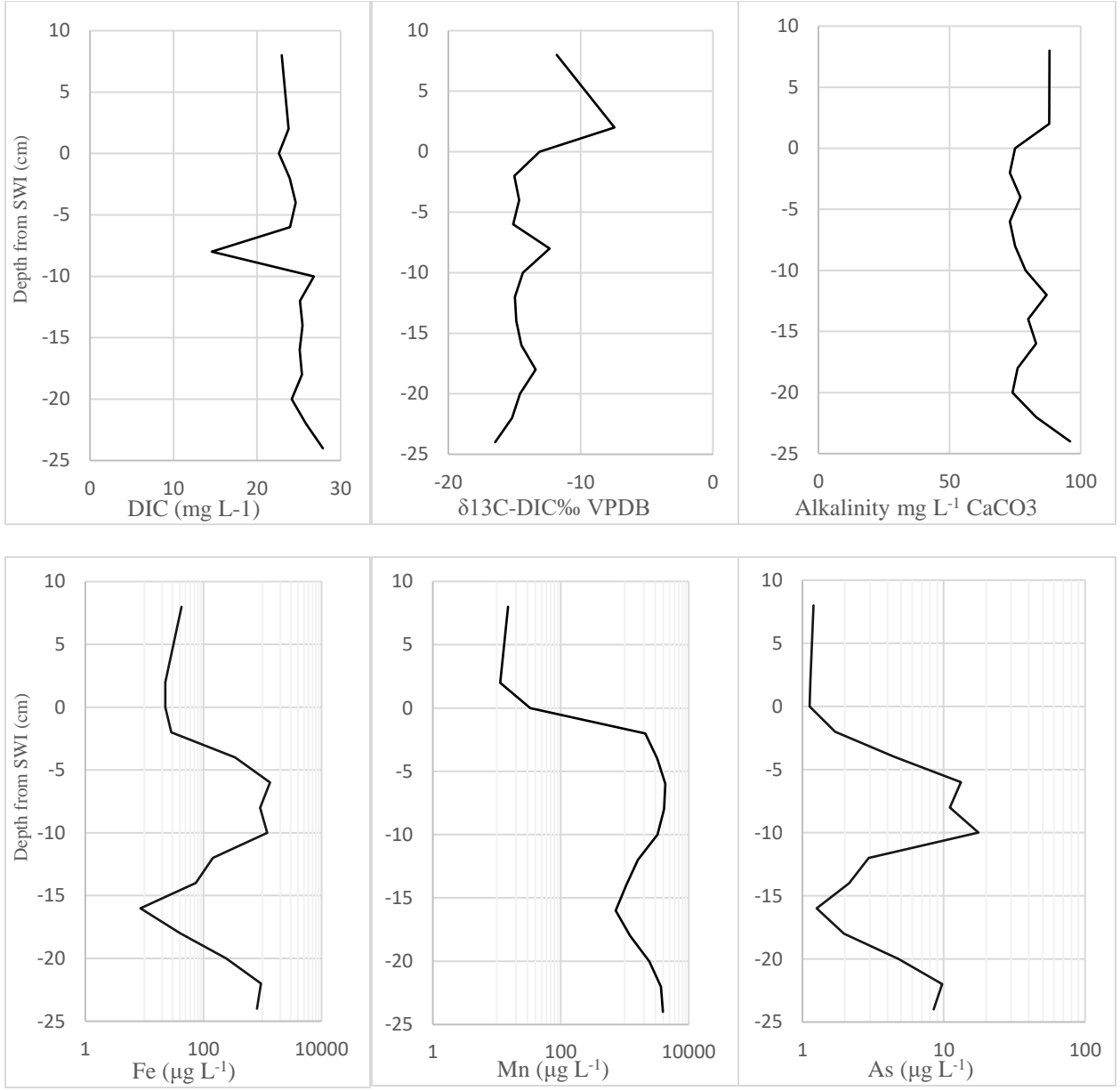


Figure 14: Peepers 20 and 21 results 0 indicates SWI, note x axis scale variance

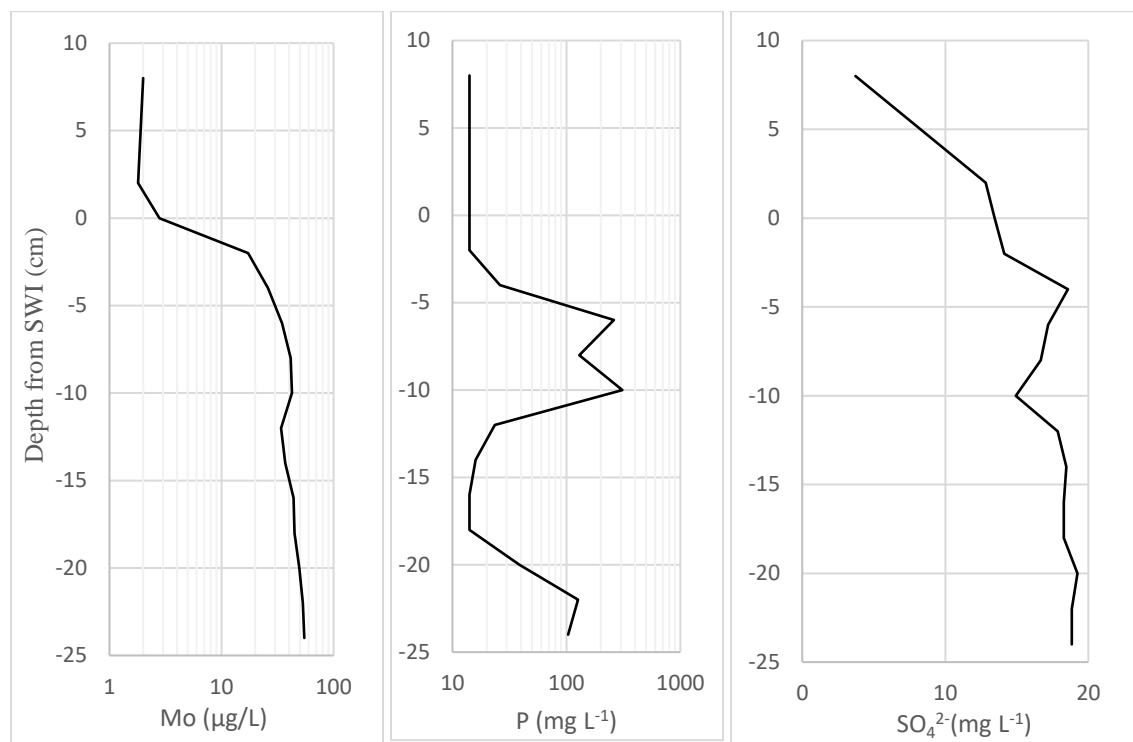


Figure 15: Peepers 20 and 21 results 0 indicates SWI, note x axis scale variance

3.2.1. Sediment core

The sediment core in Figure 16 was taken shortly after the deployment of the peepers about 10 cm downstream from the peepers. Within the sediment core, fine grain sediments make up the top 8 cm and coarse grain sediments make up the rest of the depth. This is another smaller fine grain zone towards the bottom, but it is below the reach of the peepers.



Figure 16: Sediment core from peepers 20 and 21

3.2.2. Calculated pH

Table VII shows the results for calculating pH using the carbonate equilibrium system.

Using an acid dissociation constant value (K_a) of 2.77971×10^{-7} , the carbonate equilibrium equation was set to solve for activity of hydrogen ions and then converted to pH.

Table VI: calculated pH values for peepers 20 and 21

Depth from SWI (cm)	DIC (mg C L ⁻¹)	Alkalinity as mg L ⁻¹ CaCO ₃	HCO ₃ ⁻ (mg C L ⁻¹)	H ₂ CO ₃ (mg C L ⁻¹)	pH
Surface	22.9	88	21.1	1.79	7.37
4	23.8	88	21.1	2.66	7.20
2	22.6	75	18.0	4.62	6.89
0	23.9	73	17.5	6.38	6.74
-2	24.6	77	18.5	6.15	6.78
-4	23.9	73	17.5	6.42	6.74
-6	25.4	75	18.0	7.10	6.70
-10	26.8	79	19.0	7.85	6.68
-12	25.1	87	20.9	4.26	6.99
-14	25.4	80	19.2	6.24	6.79
-16	25.1	83	19.9	5.18	6.89
-18	25.4	76	18.2	7.12	6.71
-20	24.2	74	17.8	6.40	6.74
-22	25.8	83	19.9	5.92	6.83
-24	27.9	96	23.0	4.84	6.98

The surface water was measured using a Hydrolab with a pH probe. The Hydrolab pH probe measured a value of 6.91 and was measured close to where the upper most peeper cell was positioned. This measurement was taken when the peepers were installed.

3.2.3. Peeper 20 DIC speciation

Figure 17 shows concentrations of DIC, $\text{HCO}_3^{-1}(\text{aq})$, and $\text{H}_2\text{CO}_{3(\text{aq})}$ in the BMS site. The bulk reservoir of DIC in the BMS area is consistently depleted at about -15%. This is likely due to the decay of organic matter releasing depleted CO_2 into the sediment. While dissolved oxygen was not recorded, the sediments are fine to medium grain sands allowing for easy diffusion between pore water spaces and stream water column.

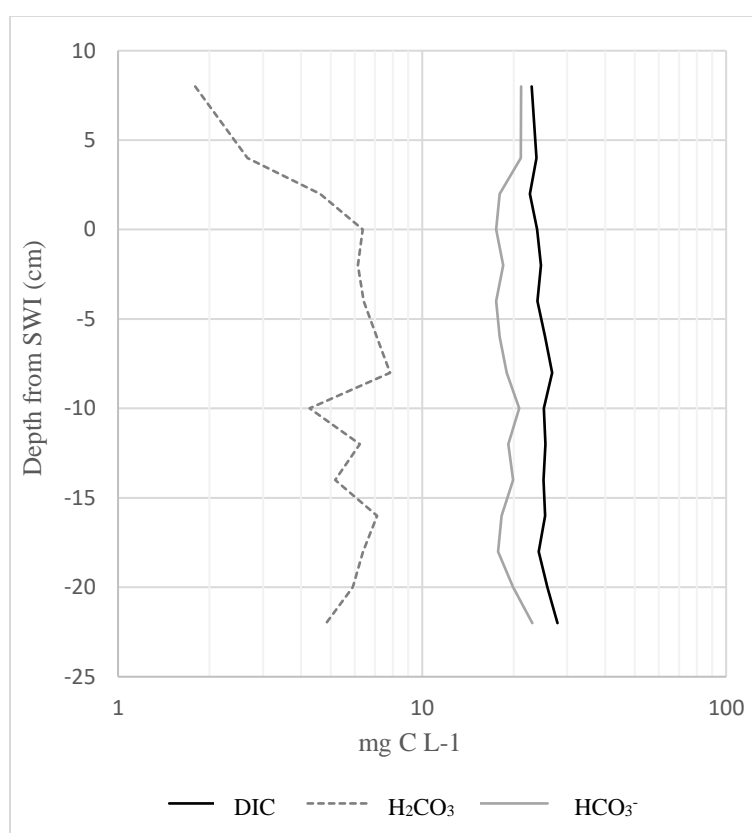


Figure 17: Filtered DIC in peeper 20

3.2.4. DIC isotope partitions

Figure 18 shows the fractionation of $\delta^{13}\text{C}$ in peeper 20. In the sediment, the bulk $\delta^{13}\text{C}$ values tend to be consistent at about -15‰.

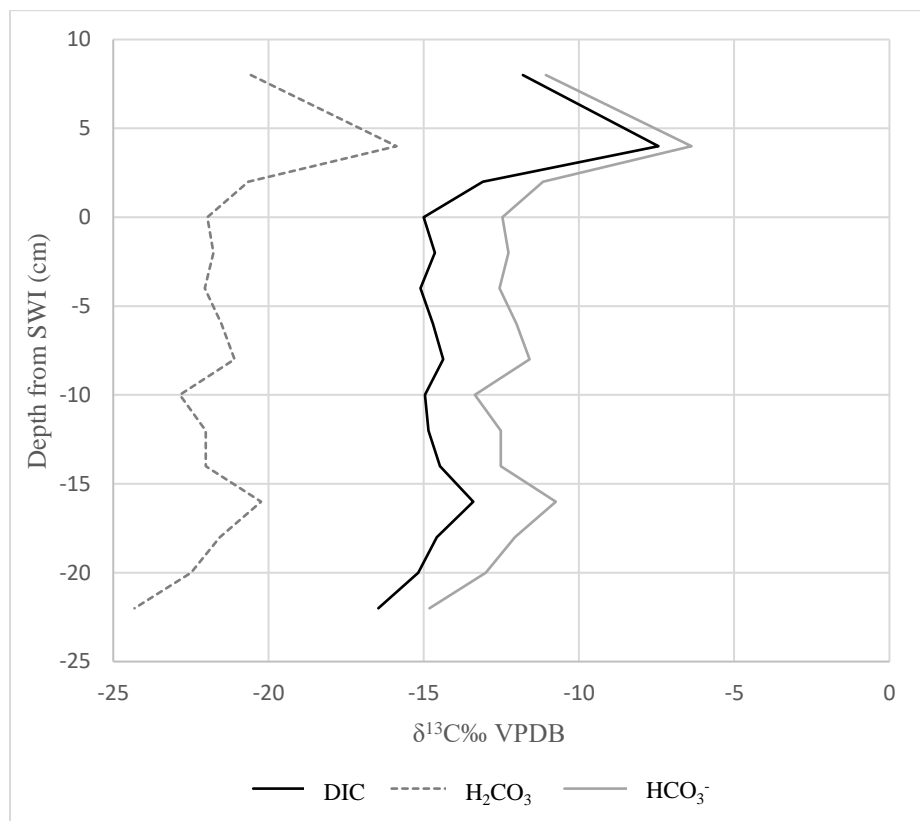


Figure 18: $\delta^{13}\text{C}$ isotope partitions in the BMS site

3.2.4.1. Diffusive flux in the BMS site

The analyte concentrations of the BMS site appear to have a diffusive flux into the stream. Figure 22 shows the higher analyte concentrations in the sediment as opposed to the stream. Using the same parameters as peeper 18, the diffusive flux into the stream was calculated for the BMS site. Table VIII shows the corresponding diffusive flux:

Table VII: Peeper 20 diffusive flux, D_o , D_s , and J are in units of ($\mu\text{g sec}^{-1} \text{cm}^{-2}$) and dC/dz in ($\mu\text{g L}^{-1} \text{cm}^{-1}$)

Analyte	Surface ($\mu\text{g L}^{-1}$)	Pore ($\mu\text{g L}^{-1}$)	dC ($\mu\text{g L}^{-1}$)	dC/dz	Porosity	D_o	D_s	J
As	1.12	17.6	-16.5	1.65	0.30	9.05×10^{-6}	8.15×10^{-7}	4.02×10^{-7}
Fe	63.1	3.38×10^3	3.32×10^3	332	0.30	5.28×10^{-6}	4.75×10^{-7}	4.73×10^{-5}
Mn	33.2	3.24×10^3	3.21×10^3	321	0.30	3.05×10^{-6}	2.75×10^{-7}	2.64×10^{-5}
DIC	2.26×10^5	2.68×10^4	-4.19×10^3	419	0.30	1.60×10^{-5}	1.44×10^{-6}	1.81×10^{-4}

3.3. Upper Blacktail Creek in Pond Sediments (Peeper 22 and 23)

Peeper 22 and 23 were placed near the BMS site in the south fork of Blacktail Creek.

This area is primarily standing water with very low rates of volumetric flow. Figure 189 shows individual solute and isotope values. Fe, Mn, and As peak between -5 and -10 cm from SWI. The surface water had a pH of 6.42, temperature of 15.88 °C, SC of 741.2 $\mu\text{S}/\text{cm}$, and ORP of -180 mV. Arsenic was below the detection limit of ICP-OES in most of the peeper cells.

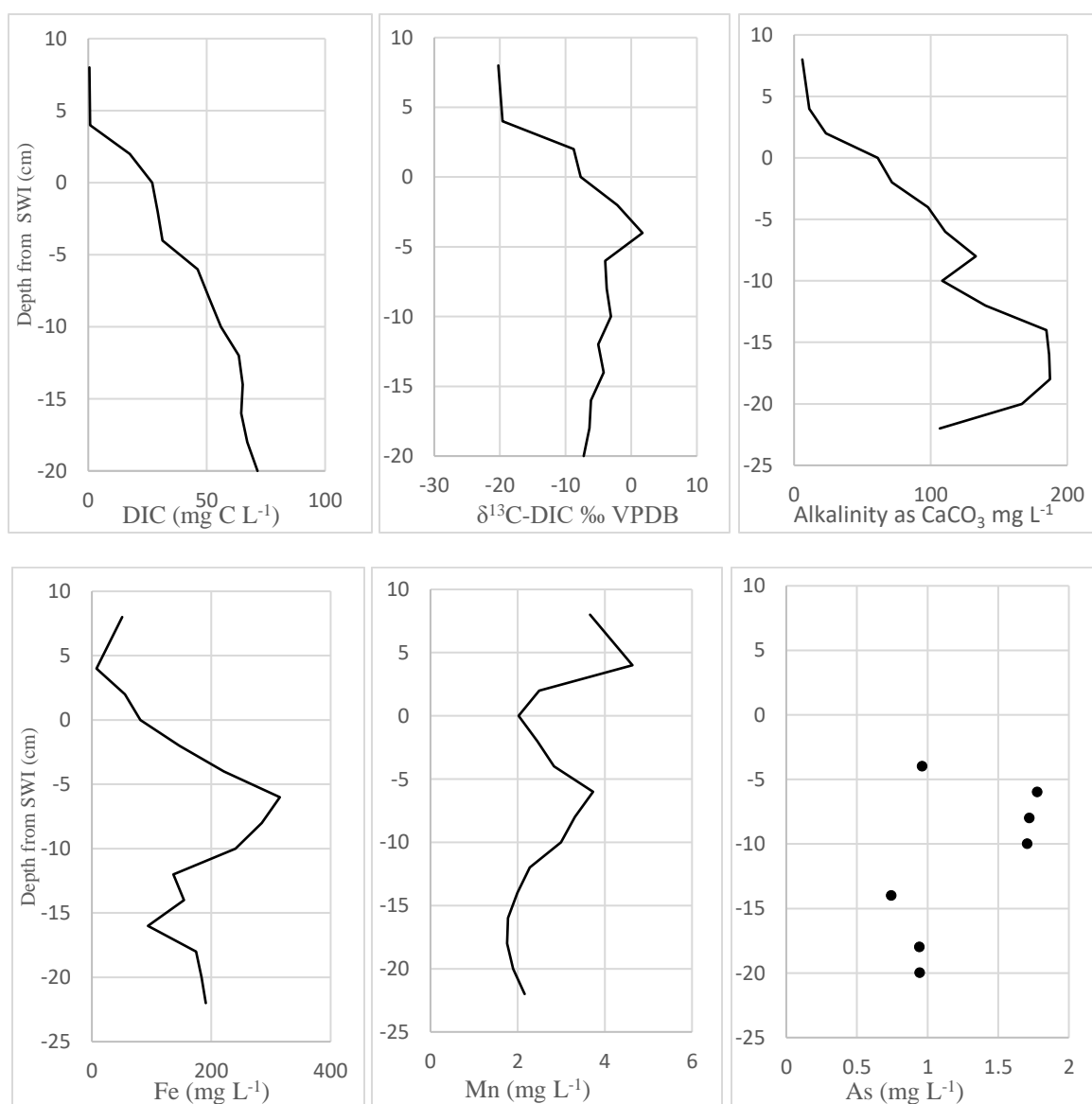


Figure 19: Peeper 22 and 23 results, 0 indicates SWI, note variance in X axes

Iron oxide precipitates were noted in some of the non-acidified samples as with peepers 18 and 19. ICP-OES analysis yielded extremely high concentrations of iron. Figure 20 shows iron oxide precipitation in surface water at the historical site.



Figure 20: Iron oxide precipitation in historical site sample

3.3.1. Sediment

The sediment core for this site was difficult to collect. Plant roots made it difficult to push the core sampler into the sediment. The small amount of sediment that was collected was very dark, organic rich and had a unique odor, possibly H_2S .

3.3.2. Calculated pH

Table VIII shows the calculated pH values for peepers 22 and 23 in the historical site.

The general trend in pH is decreasing with depth (increase in H⁺ ions).

Table VIII: Calculated pH for peepers 22 and 23

Depth from SWI (cm)	DIC (mg C L ⁻¹)	Alkalinity as (mg L ⁻¹ CaCO ₃)	HCO ₃ ⁻ (mg C L ⁻¹)	H ₂ CO ₃ (mg C L ⁻¹)	pH
surface	0.5	6.02	1.45	1.1	NA
4	0.75	11.1	2.67	2.0	NA
2	17.5	23.4	5.62	11.8	5.98
0	27.0	61.3	14.7	12.3	6.38
-2	29.3	71.7	17.2	12.1	6.45
-4	31.3	98.1	23.5	7.8	6.78
-6	46.2	111	26.5	19.6	6.43
-8	51.1	133	31.9	19.2	6.52
-10	56.0	108	26.0	30.0	6.24
-12	63.5	140	33.6	29.9	6.35
-14	65.2	185	44.3	20.9	6.63
-16	64.6	187	44.8	19.8	6.65
-18	67.2	187	45.0	22.2	6.61
-20	71.5	167	40.0	31.5	6.40
-22	error	107	25.6	NA	NA

Note: surface and 4 cm are close to detection and should be considered estimates

3.3.3. DIC speciation

Figure 21 shows the DIC isotope fractionation of the historical site with peepers 22 and 23. Alkalinity appears to drop off towards the bottom of the peeper, this could be linked to extremely anoxic conditions that promote acetoclastic methanogenesis. Cell 28 experienced too much cross contamination to be considered accurate data, so the point was omitted from the DIC.

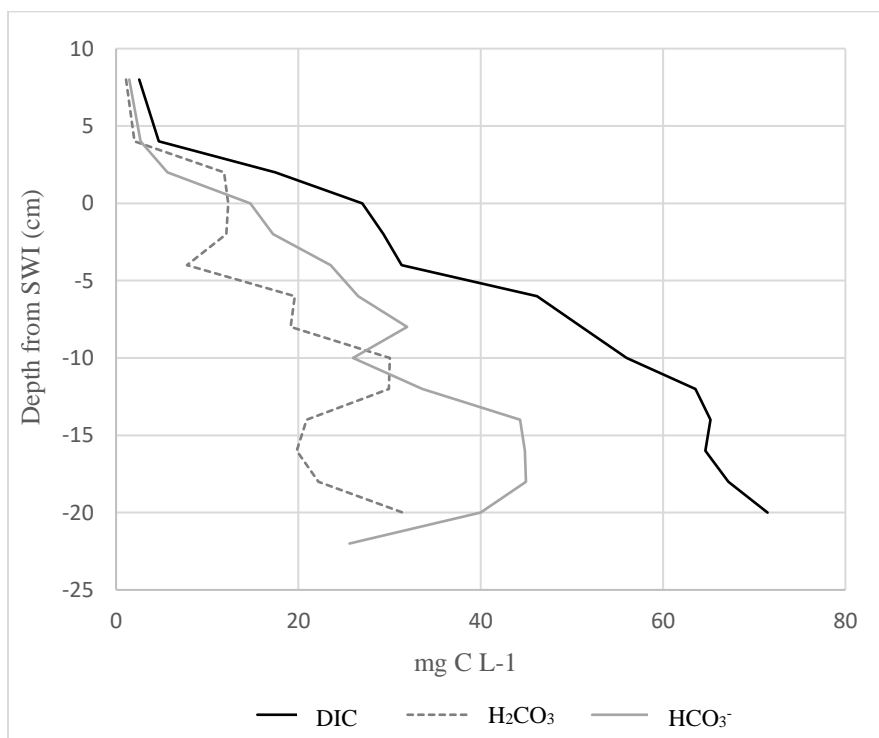


Figure 21: Peeper 23 DIC speciation in historical site

3.3.4. DIC isotope partitions

Figure 22 shows the DIC fractionation of peeper 22 and 23. These are the most enriched values in the study. The surface sample and top peeper cell measured below the detection limit, alkalinity was also very low in this section.

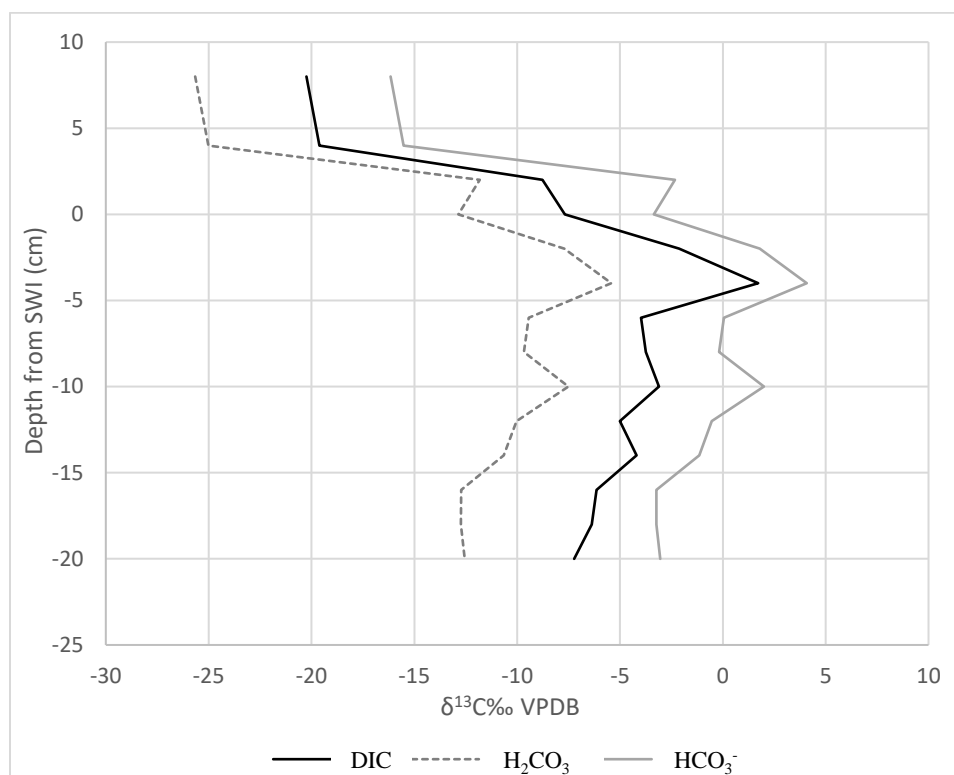


Figure 22: Isotopic compositions of DIC in peeper 23

3.3.4.1. Diffusive flux in the historical site

While ICP-MS analysis was not available for this set of samples, ICP-OES analysis was used instead. Because the ICP-OES has much higher detection limits than the ICP-MS, arsenic was below or just slightly above the detection limit. Since the detectable value(s) were within the baseline and should be considered estimated, arsenic was not used. Iron and manganese are high in the historical site and fall within the calibration range of the ICP-OES. DIC in the historical site was run the same way as the other DIC samples. Table IXX shows the diffusive flux in the historical site for Mn, Fe, and DIC.

Table IX: Peeper 23 diffusive flux where D_o , D_s , and J in units of ($\mu\text{g sec}^{-1} \text{cm}^{-2}$) and dC/dz in ($\mu\text{g L}^{-1} \text{cm}^{-1}$)

Analyte	Surface ($\mu\text{g L}^{-1}$)	Pore water ($\mu\text{g L}^{-1}$)	dC ($\mu\text{g L}^{-1}$)	dC/dz	Porosity	D_o	D_s	J
Fe	8.11×10^4	2.41×10^5	-1.60×10^5	1.60×10^4	0.30	5.28E-06	4.75E-07	2.28×10^{-3}
Mn	2.00×10^4	2.02×10^3	2.99	2.02×10^3	0.30	5.75E-06	5.18E-07	3.14×10^{-4}
DIC	2.70×10^4	5.60×10^4	-2.90×10^4	2.90×10^3	0.30	1.60E-05	1.44E-06	1.25×10^{-3}

3.4. Surface water of Blacktail Creek in between the three sites

Ten surface water samples were collected along Blacktail Creek between the BMS site and the downstream site. The purpose of this was to measure how pH, alkalinity, and DIC change downstream. The sites were chosen to show trends in DIC and DIC isotopes with distance downstream. Surface water sample locations can be seen in Figure 23.

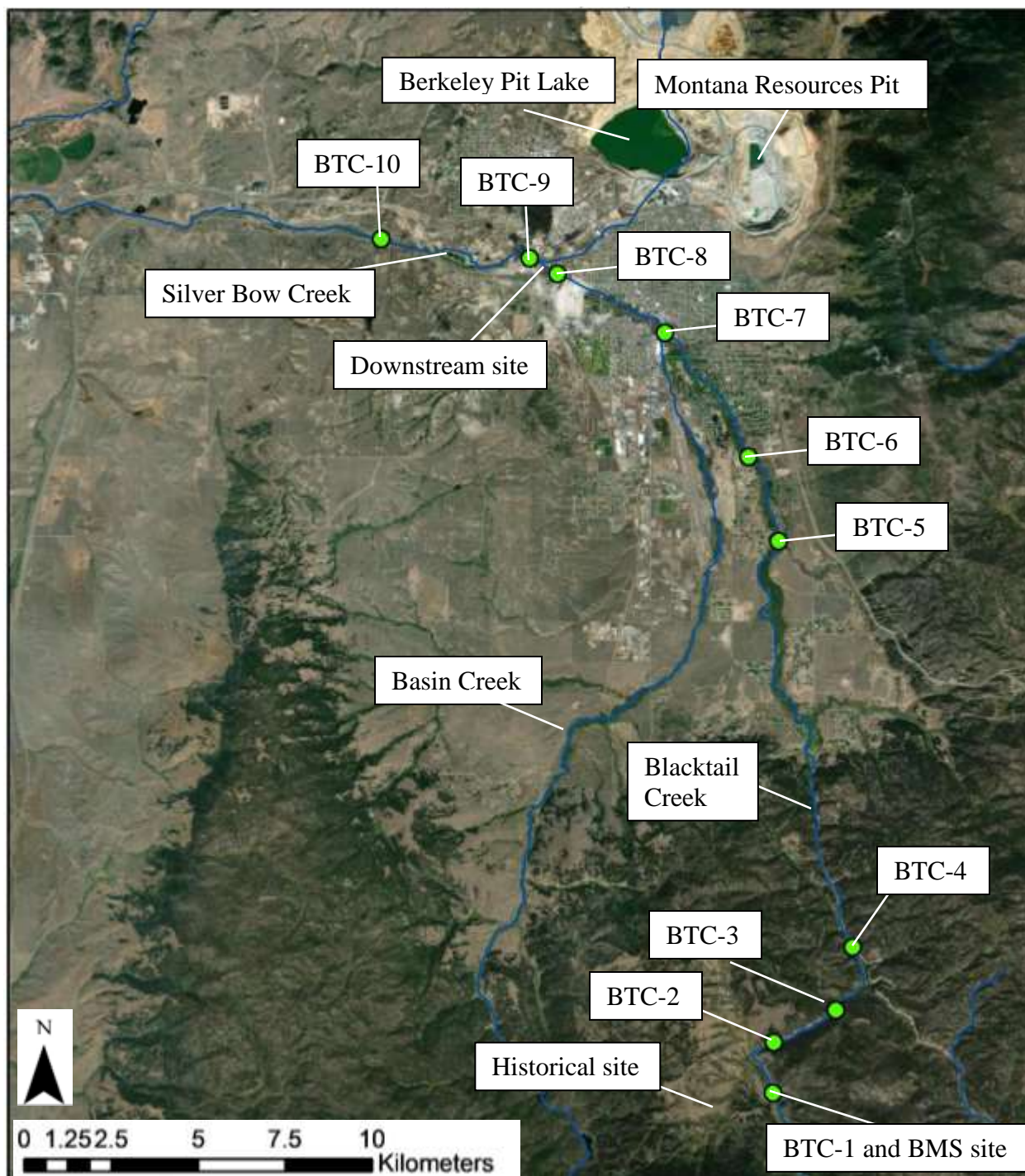


Figure 23: Map of surface water samples in between peeper sites, green points represent surface sample sites

Table X shows DIC, DIC isotopes, and alkalinity results. Surface water samples were collected on 9/18/2020, during a dry period of roughly 14 days. Based on surface water temperature, the BMS site appears to be the most alpine stream site. **Error! Reference source not found.** shows the DIC concentration and **Error! Reference source not found.** shows the isotopic composition with distance downstream. This starts in the historical site and BMS site, then ends up downstream of the wastewater treatment plant along Silver Bow Creek.

Table X: Surface water chemistry

Site name	distance (km)	pH	Temp (°C)	ORP (mV)	SC (µS/cm)	Alkalinity as CaCO ₃ (mg L ⁻¹)	DIC (mg C L ⁻¹)	δ ¹³ C-DIC ‰VPDB
Historical	0.00	6.42	15.9	-180	741	60.2	0.50	-20.2
BMS	1.30	7.69	6.87	254	257	87.4	27.4	-9.4
BTC-2	1.61	7.53	7.37	258	227	100	23.5	-9.1
BTC-3	2.75	8.19	7.82	265	196	77.0	19.8	-7.4
BTC-4	4.36	8.08	8.55	282	212	77.8	18.2	-7.1
BTC-5	13.2	7.11	14.4	157	364	84.0	21.8	-11.6
BTC-6	15.0	8.71	12.4	229	282	72.6	19.0	-9.7
BTC-7	18.3	7.94	11.1	268	325	85.0	22.2	-11.7
BTC-8	20.8	8.26	12.0	278	390	81.2	25.6	-11.6
BTC-9	21.5	7.95	14.1	269	1731	64.2	16.6	-9.0
BTC-10	24.9	8.14	14.9	297	1452	81.0	20.6	-10.5

Note: GPS coordinates of each site are in Appendix E, site photos are also included in Appendix E

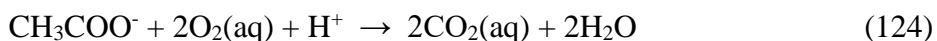
4. Discussion and Implications

4.1. Microbial reactions

Microbial processes drive many of the observations that are seen in Blacktail Creek, by influencing the dissolved geochemistry. Microbial interactions begin with dissolved organic carbon (DOC) and dissolved oxygen ($O_{2(aq)}$). A common form of DOC is in the form of acetate which is produced from heterotrophic bacteria (Gammons *et al*, 2008). Heterotrophic bacteria produce acetate as a byproduct of using pyruvate to generate ATP (Jurtshuk, 1996). Autotrophic microbes break down the acetate ions for aerobic respiration until the dissolved oxygen in the creek is completely used. Once all dissolved oxygen has been used, other microbes switch to anoxic respiration processes, starting first with denitrification, then to Fe and Mn oxide reduction and eventually sulfate reduction. Sulfate reduction happens after NO_3^- , Mn, and Fe have been sequentially used up (Alvarez-Cobelas *et al*, 1990; Helmer and Labroue, 1993; Blodau *et al*, 1998; Castro *et al*, 1999; Holowenko *et al*, 2000; Wendt-Potthoff *et al*, 2002; Harrington *et al*, 2004; Fauville *et al*, 2004; Sanchez-Espana *et al*, 2007; Gammons *et al*, 2008). Sulfate reducing bacteria (SRB) can produce H_2S which can then combine with a metal to form insoluble metal sulfides such as pyrite. After these respiration reactions are complete, microbes then switch to fermentation for metabolic energy. The most common form of fermentation is acetoclastic methanogenesis which uses the acetate anion to facilitate methanogenesis (Blodau *et al*, 1998; Whiticar *et al*, 1999; Holowenko *et al*, 2000; Parker *et al*, 2016; Gammons *et al*, 2014). This is commonly found in wetlands as they contribute about 30% of global methane emissions (Houghton *et al*, 2001).

4.1.1. Aerobic respiration

Aerobic respiration requires an abundance of $O_2(aq)$. Equation (124) shows the balanced reaction for aerobic respiration:

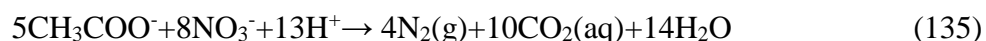


where the solvent is $H_2O(l)$. The acetate (CH_3COO^-) ion is a form of DOC that is heavily used to facilitate metabolic reactions for microbes (Alvarez-Cobelas *et al*, 1990). The upstream peeper site displays characteristics of aerobic respiration in the surface water and in the sediment based on the isotopic composition of DIC shown in Figure 18. Since the sediments in this site are sandy, this promotes rapid diffusion of atmospheric dissolved oxygen into the pore water spaces. The BMS site displays normal aerobic respiration in sandy sediments where the $\delta^{13}C$ values are around -15‰ with concentrations between 20 and 23 ppm C.

The surface water in the historical site is already anoxic as indicated by the negative ORP of -180 mV (see Table X), so microbes must use other substrates to facilitate metabolic reactions. In the downstream site, Fe and Mn spike in the sediment just below the SWI in the sediment; this can be seen in Figure 9. Concentration gradients naturally drive dissolved Fe and Mn to the surface where they can precipitate out as Fe and Mn oxides once in an aerobic environment (Blodau *et al*, 1998; Wendt-Potthoff *et al*, 2002; Sanchez-Espana *et al*, 2007). This indicates that aerobic respiration is occurring above the SWI. The historical and downstream sites do not display evidence of aerobic respiration. These two sites are anoxic and require other sources to facilitate metabolic reactions.

4.1.2. Denitrification and Dissimilatory nitrate reduction to ammonia

Nitrate is only detectable in the downstream peeper 18. Only the top two peeper cells and the surface water sample contained nitrate. Nitrite was below the detection limit in all three of the peeper sites. This indicates that nitrate is either being reduced to ammonia by dissimilatory nitrate reduction to ammonium (DNRA), or nitrate is being oxidized to $N_{2(g)}$ by denitrification in the sediment. Nitrogen could also be absent in the sediment column, but this is unlikely due to the baseflow season. Denitrification reaction releases $N_{2(g)}$ and $CO_{2(aq)}$ that will be isotopically light. Equation (135) shows denitrification:



where acetate is the electron donor (oxidized species) and nitrate is the electron acceptor (reduced species) (Helmer and Labroue *et al*, 1993). Both processes result in the consumption of nitrate from the system. DNRA and denitrification can both be occurring simultaneously. The presence of sulfate reduction that produces sulfide provides a proper electron donor to facilitate DNRA. Multiple studies have observed the process of DNRA in anoxic freshwater and anoxic marine fine grain sediments (Payne, 1973; Koike and Hattori, 1978; Kelso *et al*, 1997). DNRA is shown in the half cell reaction in Equation (146):



(Payne, 1973; Kamp *et al*, 1973; Koike and Hattori, 1978; Kelso *et al*, 1997). In the presence of H_2S , DNRA can proceed in anoxic conditions using biogenic H_2S as the electron donor.

Equation (157) shows the oxidation half-cell reaction of sulfide being oxidized. The electrons are then used to facilitate DNRA in the presence of nitrate.



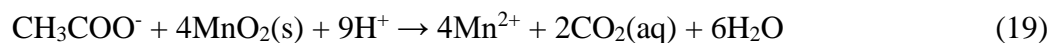
Equation 18 shows how the two half-cell reactions combine to facilitate DNRA (Kamp, 2006).



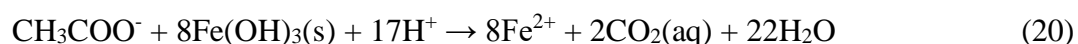
Other electron donors can be used to facilitate DNRA, but sulfide is most likely in the downstream site due to the sulfate reduction observed. No nitrite is detected in the downstream site. The upstream sites do not show any detectable species of nitrate or nitrite.

4.1.3. Iron and Manganese oxide reduction

Equation 19 shows the reduction of Mn oxide which releases isotopically light CO₂ from the breakdown of acetate



Equation 20 shows iron oxide reduction which also releases isotopically light CO₂ and also breaks down acetate (Blodau *et al*, 1998; Wendt-Potthoff *et al*, 2002; Sanchez-Espana *et al*, 2007; Gammons *et al*, 2008).



Both of these reactions facilitate electrons for anaerobic respiration and metabolic energy. Figure 9 shows the downstream site (peeper 18) has both Fe and Mn oxide reduction occurring beginning at about -5 cm. In the surface water, there is less than 0.1 mg L⁻¹ of Fe and Mn. These values increase over one hundred-fold below the SWI. This indicates that all available dissolved oxygen has been used and microbes are now using Fe and Mn reduction for respiration. Arsenate (AsO₄³⁻) adsorbs to Fe and Mn oxides, so when they are reductively dissolved the adsorbed As is released into the pore water (Peña & Torrent, 1984; Dixit & Torrent 2003).

These reactions can also be observed in the BMS site between 5 cm and 10 cm in the sediment column seen in Figure 14 and Figure 15. Characteristics of aerobic respiration can be

observed taking place in the surface water and in the peeper until 5 cm in the sediment. Below 5 cm, Fe, Mn, As, and all other solutes spike again. While the sediment in the BMS site is sandy compared to the downstream and historical sites, there is a fine grain layer in the sediment core that was collected. This is at the same depth where the solute spike occurs (-5 to -10 cm). This section and below is most likely anoxic. There is a spike in As and P likely due to the adsorption onto the iron oxides. There appears to be enough Fe and Mn to sustain anaerobic metabolism, so the next metabolic process, fermentation, does not have to take place. As with peeper 18 downstream, peeper 20 also observes As mimicking Fe and Mn due to adsorption. Arsenic and phosphorous adsorb readily to Fe and Mn oxides in the form of arsenate ($\text{AsO}_4^{3-}(\text{aq})$) and phosphate (PO_4^{3-}) (Peña & Torrent, 1984; Dixit & Hering, 2003). Peeper 20 in the BMS site does not see methanogenesis taking place.

4.1.4. Sulfate reduction

Sulfate reduction in fine grain sediments is common in aquatic environments around Montana (Shaw *et al*, 2013; Gammons *et al*; 2014; Parker *et al*, 2016). The most common type of microbial sulfate reduction reduces sulfate to sulfide, an eight-electron transfer, directed towards metabolic energy. Sulfate reducing bacteria (SRB) reduce the sulfate anion to any sulfur species between sulfate and sulfide. Sulfate reduction by bacteria is shown in Equation 21:



where the bicarbonate released is isotopically heavy (Blodau *et al*, 1998; Castro *et al*, 1999; Harrington *et al*, 2004; Fauville *et al*, 2004).

Figure 24 shows the speciation of sulfur at normal stream conditions. Sulfate is the dominant species of sulfur at these conditions. Temperature and pressure do not affect the model

significantly unless extreme hydrothermal conditions are present. The sulfide produced from bacteria is extremely unstable and will most likely precipitate out with a metal such as pyrite.

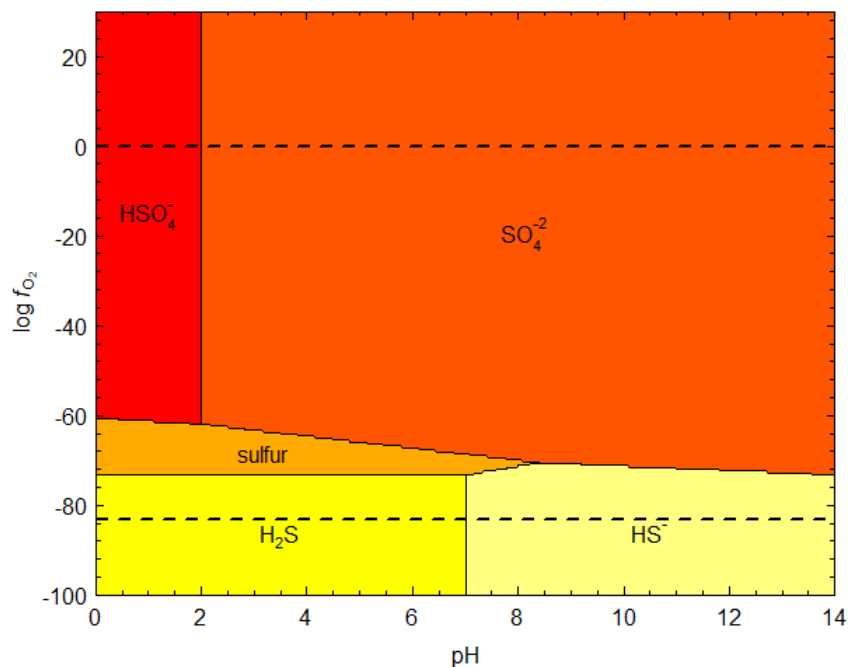


Figure 24: Sulfur speciation diagram at stream conditions (Dick, 2019)

Rader (2019) and Robertson (2019) also observe evidence of bacterial sulfate reduction in Blacktail Creek near the downstream peeper 18. Sulfide mineral precipitation could remove metals such as iron, copper, or arsenic into their most stable sulfide mineral form. The sulfide minerals can then re-oxidize and release more acid into the stream as demonstrated in the oxidation of pyrite reaction in Equation (162) where the oxidation of pyrite releases 8M of H⁺ ions into the water or sediment column:



Insoluble sulfide minerals can precipitate in the form of pyrite, chalcopyrite, sphalerite, galena, and many others.

Common sulfide mineral precipitation reactions are shown in Equations 23, 24, 25:

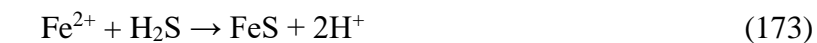


Figure 255 shows SO_4^{2-} decreasing with depth while Cl^- and F^- increase in the downstream peeper 18 site. These three anions are usually considered conservative tracers and should mimic each other's concentration gradient. SO_4^{2-} does not act conservative below the SWI at this site.

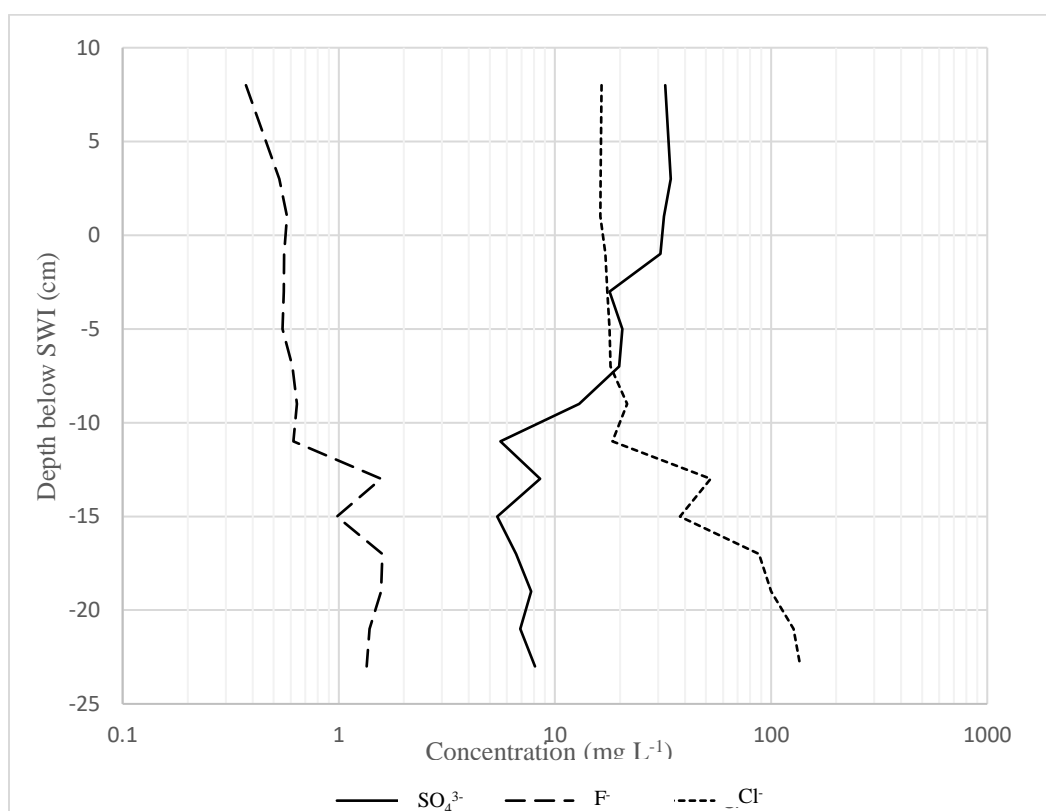


Figure 25: SO_4^{2-} , F^- , and Cl^- concentrations with depth in peeper 18

Below -10 cm in the sediment, there is not enough sulfate to sustain SRB, so microbes use Fe and Mn oxide reduction and fermentation to sustain microbial communities.

No sulfate reduction is observed in the BMS site, and shows increasing sulfate concentrations with depth in Figure 15. In alpine and sub-alpine stream environments, sulfate

usually behaves relatively conservatively in ground and surface water (Cochand *et al*, 2019). The downstream peeper 18 shows a decrease in sulfate concentration with depth indicating microbial sulfate reduction. Figure 266 shows the enrichment of $\delta^{13}\text{C}$, indicating methanogenesis (next section).

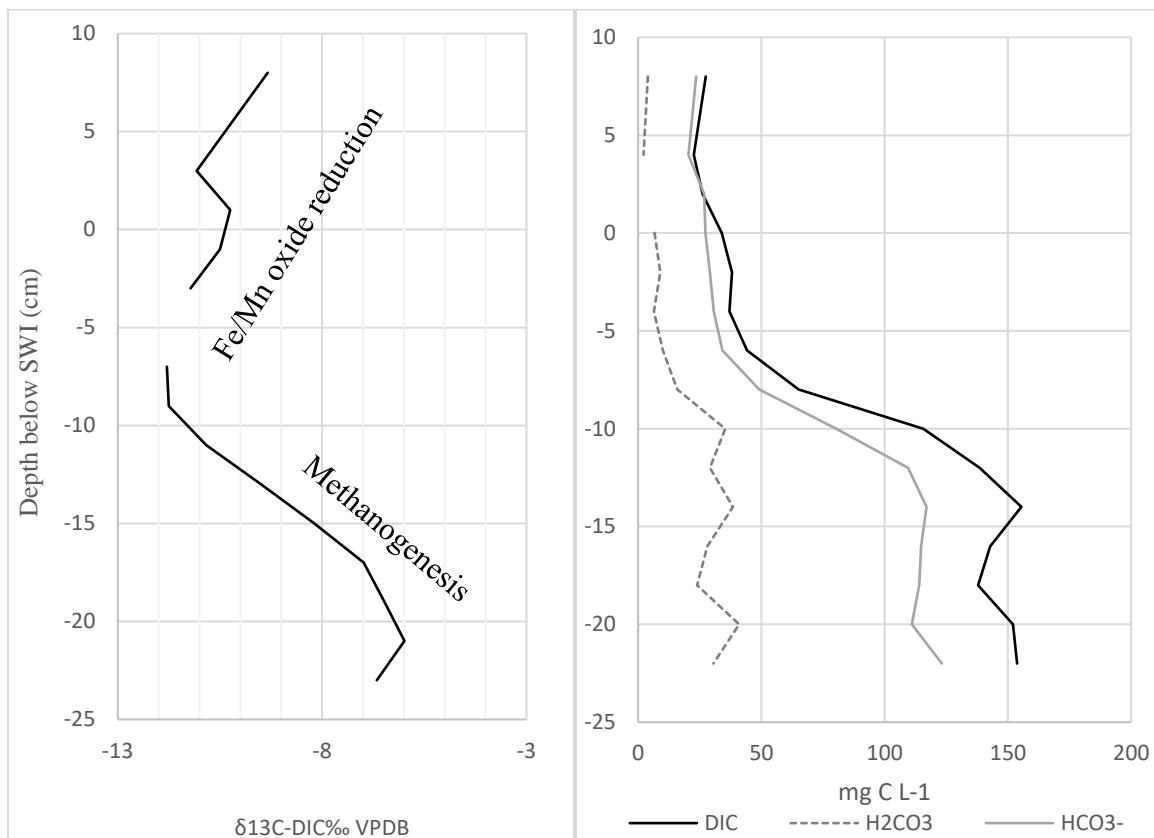


Figure 26: DIC and DIC isotopes for peeper 18 showing enrichment of inorganic carbon

Sulfide gas produced from sulfate reduction is very volatile and disperses quickly once produced in the stream bed making it difficult to sample, so no sulfide was measured.

4.1.5. Fermentation (methanogenesis)

Evidence for methanogenesis exists in the historical peeper 22 and 23 site.

Methanogenesis is microbial formation of methane by archaea in anoxic conditions.

Methanogenesis often isotopically enriches the main DIC reservoir by preferentially breaking ^{12}C bonds rather than ^{13}C . This results in very depleted methane and very enriched CO_2 (Gammons *et al.*, 2014; Parker *et al.*, 2016). This is seen in the $\delta^{13}\text{C}$ partitions in Figure 13 and Figure 18 in the downstream peeper 18 and historical peeper 23 respectively. There are multiple different metabolic pathways that methanogenesis can take, but the most likely in a wetland environment is acetoclastic methanogenesis (Blodau *et al.*, 1998; Holowenko *et al.*, 2000). This reaction cleaves the acetate anion into CO_2 and CH_4 . Methane is very volatile and difficult to sample accurately.

The peak enrichment is between the water column and 4 cm below the SWI; this is likely the soil horizon that contains most of the methanogenesis and therefore produces most of the methane. After -4 cm, the DIC becomes more depleted. This is not the decay of organic matter because that requires aerobic conditions. Methanogenesis requires anoxia, and also produces enriched CO_2 . Methanogenesis is much more likely here.

4.2. Interactions within the BMS site

In the BMS site, groundwater and surface water samples were collected a few days after sampling the peepers that were put in place. Weather conditions were considerably more winter-like in the BMS site with peepers 20 and 21 compared to when the downstream peepers 18 and 19 were sampled. Most groundwater wells were frozen and difficult to sample. The three groundwater wells that were sampled were only a maximum of 2 meters deep. The three wells were sampled on November 12, 7 days after peepers 20 and 21 were sampled in the BMS site. Only DIC and water isotopes were collected. These data are also plotted against the global meteoric water line (Craig, 1961) as well as the Butte meteoric water line (Gammons *et al.*, 2006). These data are shown in Figure 277. Groundwater wells are depleted in both δD and $\delta^{18}\text{O}$

and surface water is more enriched. The well that plots near the surface water is a flux well and has constant stream recharge.

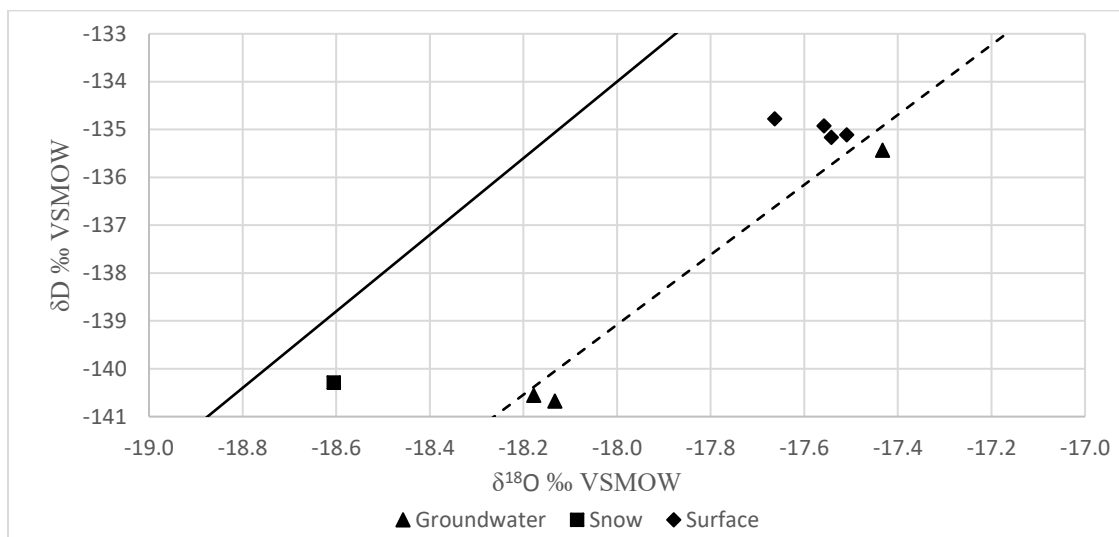


Figure 27: The local meteoric water line for Southwest Montana (dashed: Gammons *et al.*, 2006). Values for δD and $\delta^{18}O$ are compared to VSMOW. Solid line is Craig, 1961 global meteoric water line.

Ground water plots in two different regions on the local meteoric water line in the BMS site. The one well that plots further away in Figure 27 from the other two wells is a flux well and shows the transition between ground and surface water. The flux well is located in the creek. The flux well looks similar to the surface water because the groundwater and surface water are well mixed at this point, a few centimeters below the SWI. The snow sample plots close to groundwater indicating primary groundwater recharge by snow melt or rain during baseflow.

$\delta^{13}C$ isotopes and inverse concentration were plotted against each other to determine component mixing in the BMS site and how the surface water, historical peeper 23, and downstream peeper 18 compare. Figure 2828 shows the carbon isotope value $\delta^{13}C$ plotted against inverse concentration of DIC. BMS surface samples are exclusively in the BMS site. The blue surface water points are samples in between the historical/BMS and downstream site.

Higher concentrations plot left on the chart and lower concentrations plot further right. Isotope Enrichment appears at the top of the plot and depleted at the bottom. Methanogenesis and respiration both produce CO_2 . Methanogenesis produces enriched CO_2 while respiration produces a depleted CO_2 . The transition zone from Fe/Mn oxide reduction (middle section of the peeper) to methanogenesis (bottom section of the peeper) can be seen by the slope of the line changing in the downstream peeper 18. In the historical peeper 23, Dilution results in a decrease in DIC concentration which would plot further on the right. HCO_3^- fractionates more enriched compared to H_2CO_3 , and since there is much more HCO_3^- in the creek, it makes sense that the DIC would become enriched with dilution. While the BMS site does display characteristics of Fe/Mn oxide reduction, it is likely not significant enough to influence DIC concentration or isotopic composition. The historical site sees methanogenesis and also a dilution trend in the bottom section of the peeper, potentially from the influx of groundwater.

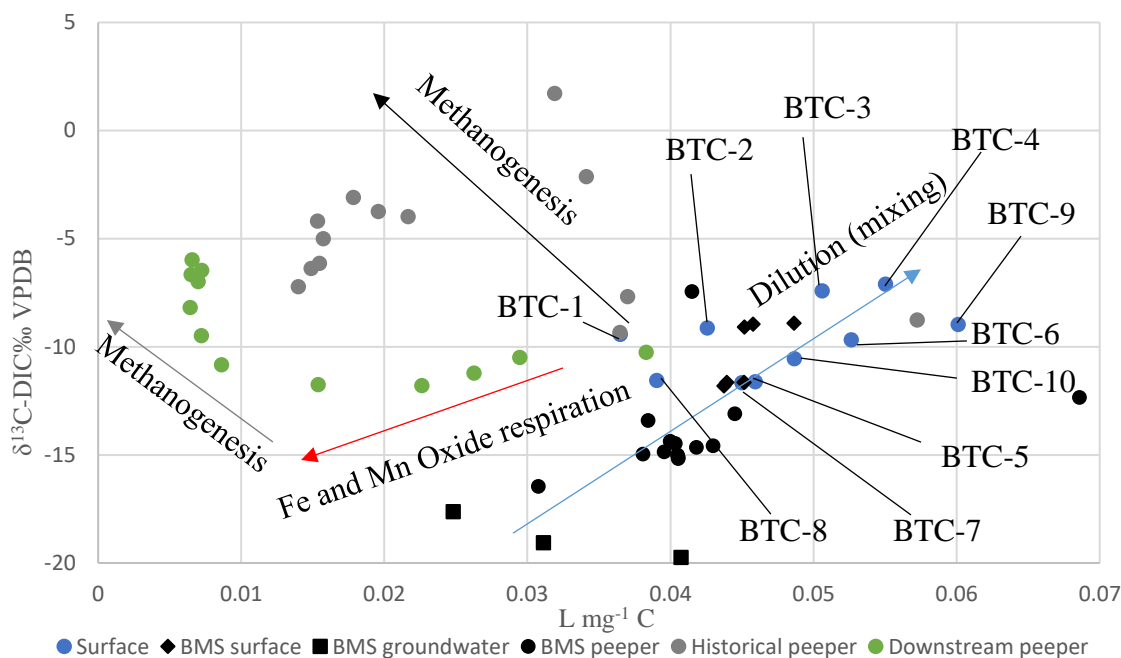


Figure 28: Endmember mixing plot of the BMS site based on inverse DIC concentrations and $\delta^{13}\text{C}$, black points represent points from the BMS site. Blue arrow shows dilution trends, red arrow shows Fe and Mn oxide reduction respiration, grey arrows represent methanogenesis

The sediments in the BMS site are coarser grained compared to the historical and downstream sites. Coarser grains allow for the groundwater to mix easily with surface water. The other peeper sites have more similar points towards the bottom of the sediment column indicating a closer relationship with groundwater than the atmosphere.

DIC derived from methanogenesis will be isotopically heavy, so in figure 30 this trend can be seen with higher DIC concentrations (closer to 0 on x axis) and more enriched isotopically (closer to 0 on y axis). Fe and Mn oxide reduction releases isotopically light CO_2 , so this trend can be seen trending towards higher DIC concentrations (closer to 0 on x axis) and more depleted isotopically (further from 0 on y axis). In the downstream peeper 18 (green dots), the transition from Fe and Mn oxide reduction to methanogenesis can be seen. The top of peeper 18 plots closer to the typical surface water DIC composition of Blacktail Creek. Figure 30 can

also help identify where other sources of water may be entering by following a dilution trend. The concentration of DIC will plot towards lower concentrations (further from 0 on the x axis), and the isotopic composition will become slightly more enriched (closer to 0 on y axis). This trend can be seen in BTC-1, BTC-2, BTC-3, and BTC-4. These sites plot in order with distance downstream along a dilution trend indicating a large influx of groundwater in the headwaters of Blacktail Creek.

4.3. Tracking DIC between the BMS site and the downstream site

Filtered DIC and $\delta^{13}\text{C}$ can be used to visualize stream DIC. The surface water is consistently about -15‰. Groundwater in the BMS site tends to be slightly more depleted in $\delta^{13}\text{C}$ at about -20‰. The deeper pore water spaces in the BMS peeper 20 tend to be more isotopically ($\delta^{13}\text{C}$) similar to the groundwater than the surface water. The uppermost peeper cells tend to be more similar to surface water. This observation suggests an isotopic transition zone. Fe and Mn oxide reduction releases isotopically depleted CO_2 into the stream and an increase with depth.

At higher the elevations in the Highlands Range, groundwater and pore water tend to be depleted in $\delta^{13}\text{C}$ (-20‰ to -15‰). The BMS site is the only peeper site out of the three that does not see a DIC concentration gradient. This is likely due to aerobic respiration in the pore water. Downstream in the valley, the surface water reflects aerobic respiration as well based on the DIC isotopic composition.

The Historical site had <1 ppm of DIC in the surface water and the top two peeper cells, but up to 71.5 ppm in the lowest peeper cell 20 cm below the surface. This implies a major concentration gradient. In the BMS site, the concentration of DIC averages about 23 ppm in the surface water during baseflow. As the surface water moves downstream, the concentration of DIC consistently decreases up to BTC-4 which is about 4.3 km downstream. The concentration

of DIC at the BTC-4 is about 18 ppm. This shows a net loss of DIC in the creek until the BTC-4. This 4.3 km section of the stream has a difference in elevation of about 200 meters. This could account for the loss of DIC as there is likely no significant source of DIC along the flow path up to this point. The DIC is likely being lost to the atmosphere as shown by the gradual enrichment from the BTC-1 (BMS) to the BTC-4.

From the BTC-6 site to the BTC-10 (flow path of about 10 km), fluctuation of DIC concentrations in the surface water range from 16.6 ppm at the BTC-9, to as high as 27.6 ppm at downstream peeper 18 site. These two sites are less than 200 m apart with the downstream site in between that had a DIC concentration of 27.41 ppm. BTC-7 is upstream of the BTC-8 and also had a relatively high concentration of DIC with a value of 22.2 ppm. The most enriched isotope value is slightly enriched (-9.7‰) at the BTC-9 site where the concentration of DIC is the lowest. This is likely due to the treated Berkeley Pit lake water being discharged into Silver Bow Creek. Water from the Berkeley Pit lake has been being discharged into Silver Bow Creek since October 1st, 2019 (Saks, 2019). Figure 29 shows the DIC profile with distance downstream in Blacktail Creek over a 25 km section. This starts in the BMS site and end about 1 km downstream of peeper 18.

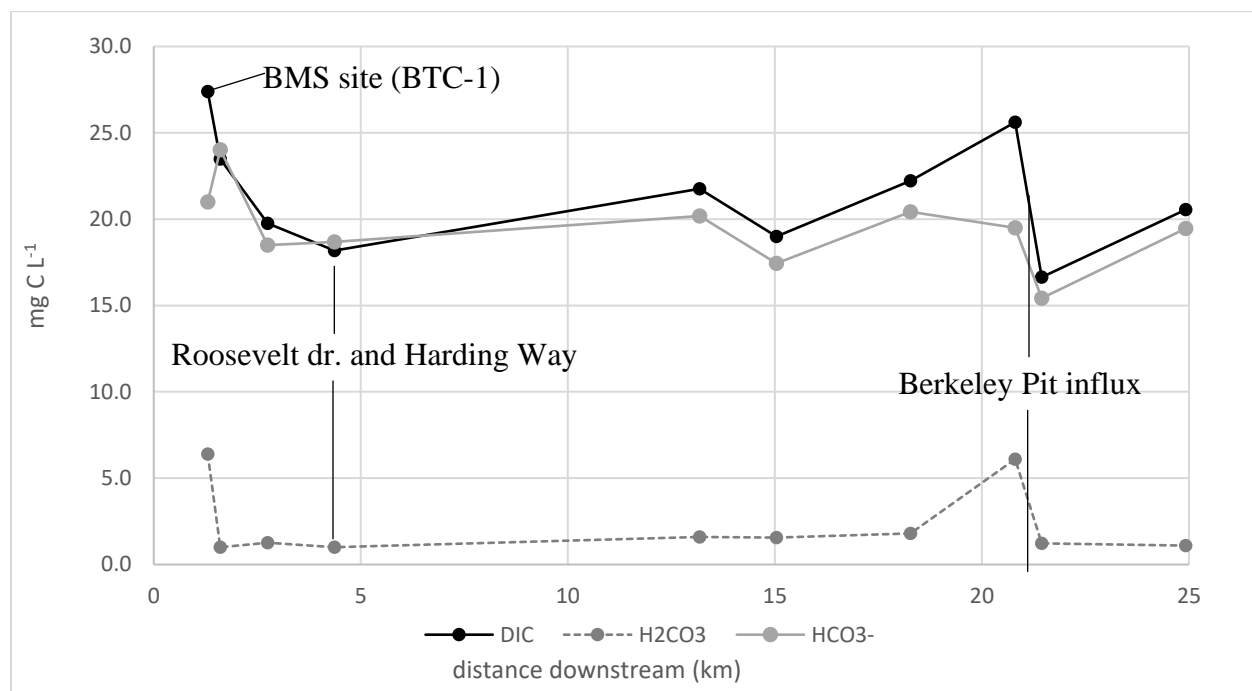


Figure 29: DIC concentrations with distance downstream from BMS site.

4.4. Predicting microbial processes based on surface DIC

The concentration of DIC in the surface water tends to be more useful than the $\delta^{13}\text{C}$ values. The peeper sites provide a baseline for different microbial processes in the subsurface and their concentration of DIC on the surface. Identifying the processes present in the sediment can help identify subsurface processes from the concentration of DIC on the surface.

The BMS peeper 20 site sees a surface value of about -10‰ and a consistent 22 mg C L⁻¹ concentration of DIC throughout the depth of the peeper, determined to be primarily aerobic respiration, with slight Fe and Mn oxide reduction. The downstream site sees a $\delta^{13}\text{C}$ value of -10‰ and a concentration of about 27 mg C L⁻¹ at the surface but the subsurface of peeper 18 increases to over 100 mg C L⁻¹ due to Fe and Mn oxide reduction from 0 to -10 cm depth and methanogenesis from -10 to -20 cm making the $\delta^{13}\text{C}$ values enriched accordingly. The historical

site has no measurable DIC in the surface, but close to 100 mg C L^{-1} in the sediment column. At the surface sites, concentration of DIC appears to be more useful than isotopic composition. Between peeper 18 and BTC-9, there is a major drop in DIC. This could be because there is more CO_2 being released from Fe and Mn oxide reduction upstream of this site and a large source of dissolved Fe and Mn that are readily being used by microbes. Sulfate reduction in the downstream site releases bicarbonate and increases alkalinity up to somewhere between peeper 18 and BTC-9 (a 200 m distance). There could be multiple different processes occurring between these two sites. Peeper 18 is experiencing all of the microbial metabolic reactions discussed except for aerobic respiration. Fe and Mn oxide reduction requires H^+ ions which raises pH and could account for the elevated pH levels seen in this section of Blacktail Creek.

5. Conclusions and Recommendations

5.1. Conclusions

The three sites in this study represent the primary environmental constituents of Blacktail Creek: sub-alpine, wetland, and valley superfund site. This project compared the three different sections of the creek with regard to DIC concentration and $\delta^{13}\text{C}$ and correlated them to effects on metals and other solutes. These three sites have different primary microbial interactions that increase DIC concentration but can either enrich or deplete the $\delta^{13}\text{C}$ values. The following bullet points are the primary conclusions for this project:

- Microbial redox reactions have a measurable effect on DIC and $\delta^{13}\text{C}$.
- The BMS site shows some Fe and Mn oxide reduction, but primarily aerobic respiration.
- The downstream site has the most microbial redox reactions taking place: Bacterial sulfate reduction, Fe and Mn oxide reduction, and methanogenesis.
- The dominant microbial process in the historical site is methanogenesis.
- Dilution trends, and microbial processes can be seen by plotting reciprocal DIC concentration against $\delta^{13}\text{C}$.
- Reciprocal DIC concentration plotted against $\delta^{13}\text{C}$ can be a useful tool in identifying different components of DIC in Blacktail Creek and can also be used in other aquatic systems.
- Sources of DIC in the valley tend to be derived from microbial anaerobic redox reactions while DIC in the BMS site is mostly derived from microbial aerobic respiration.

- Blacktail Creek is more influenced by microbial interactions in the valley superfund site (downstream site), but more influenced by groundwater and atmospheric interactions in the sub-alpine portion (BMS).

DIC is affected by all of the processes mentioned above. These processes are easy to identify and should be studied further by using similar methods.

5.2. Future work

This project primarily serves as a foundation for future projects. Some potential future research ideas are suggested below:

- Identify bacterial sulfate reduction in the historical site.
- Quantify the amount of H₂S being produced from bacterial sulfate reduction and the rate of insoluble metal sulfide precipitation in the LAO superfund site.
- Quantify methane in historical site for concentration and isotopic composition.
- Determine how upwelling or downwelling of water in sediment column influences peeper data.
- Compare different pore water chemistry sites along Basin Creek, which flows adjacent to Blacktail Creek.

Continuing to study the hydrogeochemical processes that affect Blacktail Creek provide knowledge on how to restore the historically contaminated aquatic system.

6. References

- Ågren GI, Bosatta E, & Balesdent J (1996) Isotope discrimination during decomposition of organic matter: A theoretical analysis. *Soil Science Society of America Journal*. 60(4), 1121-1126.
- Alvarez-Cobelas M, Rubio A, Velasco JL (1990) Chemical limnology of a hypertrophic gravel-pit lake. *Annales de Limnologie ANLIB3*, 26, 97-108.
- Balistrieri LS, Nimick DA, & Mebane CA (2012) Assessing time-integrated dissolved concentrations and predicting toxicity of metals during diel cycling in streams. *Science of the Total Environment*, 425, 155-168.
- Benner, S., Smart, E., and Moore, J., 1995, Metal behavior during surface-groundwater interaction, Silver Bow Creek, Montana, *Environmental Science and Technology*, v. 29, p. 1789–1795.
- Blodau C, Hoffman S, Peine A, Peiffer S (1998) Iron and sulfate reduction in the sediments of acidic mine lake 116 (Brandenburg, Germany): Rates and geochemical evaluation. *Water Air Soil Poll.* 108, 249-270.
- Bridgham SD, Cadillo-Quiroz H, Keller JK, & Zhuang Q (2013) Methane emissions from wetlands: biogeochemical, microbial, and modeling perspectives from local to global scales. *Global Climate Change Biology*, 19, 1325-1346.
- Castro JM, Wielinga BW, Gannon JE, Moore JN (1999) Stimulation of sulfate-reducing bacteria in lake water from a former open-pit mine through addition of organic wastes. *Water Environ. Res.* 71, 218-223.

Clark ID, & Fritz P (1997) *Environmental Isotopes in Hydrogeology*. New York, New York: CRC Press.

Cochand M, Christe P, Ornstein P, & Hunkeler D (2019) Groundwater storage in high alpine catchments and its contribution to streamflow. *Water Resources Research*, Volume(4), 2613-2630.

Comyn-Platt E. (2018) Carbon budgets for 1.5 and 2 °C targets lowered by natural wetland and permafrost feedbacks. *Nature*, 11(8), 568-573.

Craig H (1961) Isotopic variations in meteoric waters. *Science*, 133(3465), 1702-1703.

Devito K J, & Dillon PJ (1993) The influence of hydrologic conditions and peat oxia on the phosphorus and nitrogen dynamics of a conifer swamp. *Water Resources Research*, 29(8), 2675-2685.

Dick J (2019) CHNOSZ: Thermodynamic calculations and diagrams for geochemistry. *Frontiers in Earth Science*, 7(180), 1-18.

Dixit S & Hering JG (2003) Comparison of arsenic (V) and arsenic (III) sorption onto iron oxide minerals: implications for arsenic mobility. *Environmental Science and Technology*, 37(18), 4182-4189.

Eby GN (2016) *Principles of Environmental Geochemistry* (2 ed.). Long Grove, IL, USA: Waveland Press, Inc.

EPA (2018) Draft surface water technical impracticability evaluation, Butte Priority Soils Operable Unit, Silver Bow Creek/Butte Area NPL Site, Butte, Montana, 3038 p.

- Fauville AB, Mayer R, Frömmichen R, Friese K, Veizer J (2004) Chemical and isotopic evidence for accelerated bacterial sulphate reduction in acid mining lakes after addition of organic carbon: laboratory batch experiments. *Chem. Geol.* 204, 325-344.
- Fetter CW (2001) *Applied Hydrogeology*, 4th Ed., Prentice-Hall, Inc., Upper Saddle River, New Jersey, 598 p.
- Gammons C H, Henne W, Poulson S R, Parker S R, Johnston T B, Dore J E, & Boyd E S (2014) Stable isotopes track biogeochemical processes under seasonal ice cover in a shallow, productive lake. *Biogeochemistry*, 120, 359-379.
- Gammons C H, Poulson S R, Pellicori, D A, Reed P J, & Roesler A J (2006) The hydrogen and oxygen isotopic composition of precipitation, evaporated mine water, and river water in Montana, USA. *Journal of Hydrology*, 328(1-2), 319-330.
- Gammons C, Nimick D, & Parker S (2015) Diel cycling of trace elements in streams draining mineralized areas—a review. *Applied Geochemistry*, 57, 35-44.
- Gammons CH, Harris LN, Castro JM, Cott PA, & Hanna BW (2008) Creating lakes from open pit mines: processes and considerations, with emphasis on northern environments. *Canadian Technical Report of Fisheries and Aquatic Sciences* 2826, 1-110.
- Gammons CH, Nimick DA, Parker SR, Cleasby TE, McCleskey RB (2005) Diel behavior of Fe and other heavy metals in a mountain stream with acidic to neutral pH: Fisher Creek, Montana, USA. *Geochimica. Cosmochimica. Acta* 69, 2505-2516.
- Harrington JG, Wangerud K, Fundingsland SD (2004) Restoration of ecosystems and long-term stabilization of initially acidic pit lakes, Gilt Edge Mine Superfund Site, South Dakota. *Proc. Tailings and Mine Waste '04*, Taylor & Francis Group, London, pp. 399-406.

- Helmer C, Labroue L (1993) Denitrification in gravel-pit lakes. *Hydrobiologia* 252, 35- 44.
- Hesslein RH (1976) An in situ sampler for close interval pore water studies. *Limnology and Oceanography*, 21(6), 912-914.
- Hill A R, & Duval T P (2009) Beaver dams along an agricultural stream in southern Ontario, Canada: their impact on riparian zone hydrology and nitrogen chemistry. *Hydrological Processes*, 23, 1324-1336.
- Houghton JT, Ding Y, Griggs DJ, Noguer M, van der Linden PJ, Dai X, Maskell K, & Johnson CA. (2001) Projections of future climate change, Climate Change 2001: The scientific basis. Contribution of Working Group I to the Third Assessment Report of the Intergovernmental Panel on Climate Change, 881.
- Holowenko FM, MacKinnon MD, Fedorak PM (2000) Methanogens and sulfate-reducing bacteria in oil sands fine tailings waste. *Can. J. Microbiol.* 46, 927-937.
- Jurtshuk, P. (1996). *Medical Microbiology*. Galveston, TX: University of Texas Medical Branch at Galveston.
- Kamp A, Stief P, & Schultz-Vogt HN (2006) Anaerobic sulfide oxidation with nitrate by a freshwater beeggiatoa enrichment culture. *Applied and Environmental Microbiology*, 72(7), 4755-4760.
- Karolyte R, Serno S, Johnson G, & Gilfillan SM (2017) The influence of oxygen isotope exchange between CO₂ and H₂O in. *Applied Geochemistry*, 84, 173-186.

- Kelso B, Smith R V, Laughlin R, & Lennox D (1997) Dissimilatory nitrate reduction in anaerobic sediments leading to river nitrite accumulation. *Applied Microbiology*, 63, 4679-4685.
- Koch R, Capoccia S, & Mariano M (2017) Macroinvertebrates as Indicators of Water Quality in Blacktail Creek. *Intermountain Journal of Sciences*, 23, 110-111.
- Koike & Hattori (1978) Denitrification and ammonia formation in anaerobic coastal sediments. *Applied Environmental Microbiology*, 35, 278-282.
- Lehn GO, Jacobson AD, Douglas TA, McClelland JW, Barker AJ, & Khosh MS (2017) Constraining seasonal active layer dynamics and chemical weathering reactions occurring in North Slope Alaskan watersheds with major ion and isotope ($\delta^{34}\text{S}_{\text{SO}_4}$, $\delta^{13}\text{C}_{\text{DIC}}$, $^{87}\text{Sr}/^{86}\text{Sr}$, $\delta^{44}/^{40}\text{Ca}$, and $\delta^{44}/^{42}\text{Ca}$) measurements. *Geochimica Cosmochimica Acta*, 217, 399-420.
- Li YH, & Gregory S (1974) Diffusion of ions in sea water and in deep-sea sediments. *Geochimica et Cosmochimica Acta*, 38, 703-714.
- Metesh J, & Madison J (2004) Summary of investigation, Upper Silver Bow Creek, Butte, Montana: Montana Bureau of Mines and Geology Open-File Report 507, 7 p.
- Norman E (2020) Hydrologic response of headwater streams restored with beaver dam analog structures. M.S. Thesis, Montan Tech, Butte, MT.
- Parker SR, West RF, Boyd ES, Feyhl-Buska J, Gammons CH, Johnston TB, Poulson SR (2016) Biogeochemical and microbial seasonal dynamics between water column and sediment

- processes in a productive mountain lake: Georgetown Lake, MT, USA. *Journal of Geophysical Research*, 121(8), 2064-2081.
- Payne WJ (1973) Reduction of nitrogenous oxides by microorganisms. *Bacteriological Reviews*, 37, 409–452.
- Pena F & Torrent J (1984) Relationships between phosphate sorption and iron oxides in Alfisols from a river terrace sequence of Mediterranean Spain. *Geoderma*, 33(4), 283-296.
- Pollock M, Beechie T, Wheaton J, Jordan C, Bouwes N, Weber N, & Voke C (2014) Using Beaver Dams to Restore. *Bioscience*, 64, 279-290.
- Puttock A, Graham HA, Cunliffe AM, Elliot M, & Brazier RE (2017) Eurasian beaver activity increases water storage, attenuates flow and. *Science of the Total Environment*, 576, 430-443.
- Rader R (2019) Geochemistry of metals and nutrients in fine-sediment pore water in Blacktail and Silver Bow Creeks, Butte, Montana. M.S. Thesis. Montana Tech, Butte, MT.
- Robertson Isaiah (2019) Limitations to photosynthesis in Silver bow and Blacktail Creeks M.S. Thesis. Montana Tech, Butte, MT.
- Sanchez-Espana J, Pamo EL, Santorimia E, Diez M (2007) Different types of hydrochemical stratification in the acidic mine pit lakes of the Iberian Pyrite Belt. *Proc. V. M. Goldschmidt Conf.*, Cologne, Germany, p. A871.
- Saks N (2019) Butte reaches superfund milestone, releasing Berkeley Pit water into Silver Bow Creek. *Montana Public Radio*.

- Shaw GD, White ES, & Gammons CH (2013) Characterizing groundwater–lake interactions and its impact on lake water quality. *Journal of Hydrology*, 492, 69-78.
- Tanaka M, Takahashi Y, Yamaguchi N, Kyoung-Woong K, Zheng G, & Sakamitsu M (2013) The difference of diffusion coefficients in water for arsenic compounds at various pH and its dominant factors implied by molecular simulations. *Geochimica et Cosmochimica Acta*, 105, 360-371.
- Tucci N J (2014) Stream characterization of Blacktail and Silver Bow Creeks, a continuous tracer injection investigation conducted during baseflow conditions in an urban area impacted by mining: Butte, Montana. Montana Bureau of Mines and Geology Report of investigation 22.
- Tucci NJ (2014) Tailings/Impacted Sediment Delineation of the Diggings East, Blacktail Creek Berm, and Northside Tailings Areas. Butte, MT: MBMG. Montana Bureau of Mines and Geology, Butte.
- Tucci N, & Icopini G (2012) Geochemical and Hydrogeologic Investigation of Groundwater Impacted by Wastes Left in Place in the Butte Priority Soils Operable Unit Butte, MT Montana Bureau of Mines and Geology, GWIC open-file 613.
- Wegener P, Covino T, & Wohl E. (2017) Beaver-mediated lateral hydrologic connectivity, fluvial carbon and nutrient flux, and aquatic ecosystem metabolism. *Water Resources Research*, 4606-4623.

- Wendt-Potthoff K, Frommchen R, Herzsprung P, Koschorrek M (2002) Microbial Fe(III) reduction in acidic mining lakes sediments after addition of an organic substrate and lime. *Water Air Soil Pollut.* 2, 81–96.
- Westbrook C, Cooper DJ, & Butler DR (2013) Beaver Hydrology and Geomorphology. *Treatise on Geomorphology*, 12, 293-306.
- Whiticar MJ (1999) Carbon and hydrogen isotope systematics of bacterial formation and oxidation of methane. *Chemical Geology*, 161(1-3), 294-314.
- Young ED, Galy A, & Nagahara H (2002) Kinetic and equilibrium mass-dependent isotope fractionation laws in nature and their geochemical and cosmochemical significance. *Geochimica et Cosmochimica Acta*, 66(6), 1095-1104.
- Zhang J, Quay PD, & Wilbur DO (1995) Carbon isotope fractionation during gas-water exchange and dissolution of CO₂. *Geochimica et Cosmochimica Acta*, 59(1), 107-114.
- Zhang Q, Jin Z, Zhang F, & Xiao J (2015) Seasonal variation in river water chemistry of the middle reaches of the Yellow River and its controlling factors. *Journal of Geochemical Exploration*, 156, 101-113.

7. Appendix A: Peeper sampling plans

Table XI: Peeper 20 and 21 sampling layout

Cell	ICP-MS/OES	IC	Alkalinity	DIC	PO ₄ ³⁻
1					
2					
3					
4					
5					
6					
7					
8					
9					
10					
11					
12					
13					
14					
15					
16					
17					
18					
19					
20					
21					
22					
23					
24					
25					
26					
27					
28					

Table XII: Peeper 18 and 19 sampling layout

Cell	ICP-MS/OES	IC	Alkalinity	DIC	H ₂ S
1					
2					
3					
4					
5					
6					
7					
8					
9					
10					
11					
12					
13					
14					
15					
16					
17					
18					
19					
20					
21					
22					
23					
24					
25					
26					
27					
28					

Table XIII: Peeper 22-23 sampling layout

Cell	ICP-OES	Alkalinity	DIC
0	█	█	█
1	█		
2		█	█
3	█		
4		█	█
5	█		
6		█	█
7	█		
8		█	█
9	█		
10		█	█
11	█		
12		█	█
13	█		
14		█	█
15	█		
16		█	█
17	█		
18		█	█
19	█		
20		█	█
21	█		
22		█	█
23	█		
24		█	█
25	█		
26		█	█
27	█		
28		█	█

8. Appendix B: DIC results by peeper

Table XIV: Peeper 18 and 19 results corrected for dilution

Cell	Alkalinity CaCO ₃ mg L ⁻¹	DIC mg C L ⁻¹	Std. Dev mg C L ⁻¹	δ ¹³ C-DIC ‰ VPDB	Std. Dev. ‰
0	98.1	27.4	1.3	-9.33	1.23
1	85.0				
2		22.6	0.2	-11.1	0.33
3	112				
4		26.1	0.2	-10.3	0.17
5	114				
6		33.9	0.4	-10.5	0.14
7	121				
8		38.1	1.3	-11.2	0.12
9	128				
10		37.0	0.5	Error	1.00
11	142				
12		44.2	0.6	-11.8	0.52
13	205				
14		65.0	1.1	-11.8	0.09
15	335				
16		115	0.9	-10.8	1.00
17	456				
18		138	2.1	-9.5	0.63
19	487				
20		155	1.6	-8.19	1.09
21	478				
22		143	1.6	-6.99	0.55
23	475				
24		138	2.2	-6.47	0.31
25	463				
26		152	2.1	-5.98	0.25
27	513				
28		154	4.1	-6.66	0.93
blank	NA	0.49	0.1	-20.3	2.84

Table XV: peeper 20 and 21 DIC results, corrected for dilution

Cell	Alkalinity CaCO ₃ mg L ⁻¹	DIC mg C L ⁻¹	Std. Dev mg C L ⁻¹	δ ¹³ C-DIC ‰ VPDB	Std. Dev. ‰
8	88	22.9	0.71	-11.8	0.07
5	88				
4		23.8	0.31	-7.44	0.31
3	75				
2		22.6	0.29	-13.1	0.29
1	73				
0		23.9	0.21	-15.0	0.27
-1	77				
-2		24.6	0.26	-14.7	0.50
-3	73				
-4		23.9	0.25	-15.1	0.09
-5	75				
-6		NA	2.24	-12.3	2.77
-7	79				
-8		26.8	0.66	-14.4	0.29
-9	87				
-10		25.1	0.23	-15.0	0.19
-11	80				
-12		25.4	0.10	-14.9	0.14
-13	83				
-14		25.1	0.15	-14.5	0.08
-15	76				
-16		25.4	0.10	-13.4	0.24
-17	74				
-18		24.1	0.20	-14.6	0.18
-19	83				
-20		25.8	0.23	-15.2	0.29
-21	96				
-22		27.9	0.08	-16.5	0.15
blank	NA	0.47	0.02	-22.6	3.42

Table XVI: Peeper 22 and 23 DIC and alkalinity results, corrected for dilution

Depth from SWI (cm)	Alkalinity CaCO ₃ mg L ⁻¹	DIC mg C L ⁻¹	Std. Dev mg C L ⁻¹	δ ¹³ C-DIC ‰ VPDB	Std. Dev. %
8	12.0	0.48	0.03	-20.2	1.72
5					
4	22.2	0.79	0.02	-19.6	1.21
3					
2	46.8	17.5	0.45	-8.77	0.27
1					
0	123	27.0	0.23	-7.68	0.04
-1					
-2	144	29.3	0.32	-2.13	0.11
-3					
-4	196	31.3	0.65	1.72	0.10
-5					
-6	221	46.2	1.03	-3.98	0.14
-7					
-8	266	51.1	0.13	-3.74	0.02
-9					
-10	217	56.0	0.28	-3.10	0.06
-11					
-12	280	63.5	0.49	-5.01	0.04
-13					
-14	369	65.2	0.68	-4.19	0.06
-15					
-16	374	64.6	0.44	-6.14	0.05
-17					
-18	375	67.2	0.14	-6.38	0.11
-19					
-20	333	71.5	1.10	-7.22	0.15
-21					
-22	213	Error	Error	Error	Error
blank	NA	<0.2	NA	NA	NA

9. Appendix C: Ion Chromatography

Table XVII: Ion Chromatography peeper 18 and 19, corrected for dilution

Cell	Chloride (mg Cl ⁻ L ⁻¹)	Sulfate (mg SO ₄ ²⁻)	Fluoride (mg F ⁻ L ⁻¹)	Nitrite (mg NO ₂ ⁻ L ⁻¹)	Nitrate (mg NO ₃ ⁻ L ⁻¹)	Phosphate (mg PO ₄ ³⁻ L ⁻¹)
0	16.5	32.4	0.4	<0.03	0.85	0.06
1	16.2	34.3	0.5	<0.06	0.49	<0.12
3	16.2	31.9	0.6	<0.06	0.47	<0.15
5	17.1	30.8	0.6	<0.06	<0.05	0.13
7	17.5	17.9	0.6	<0.05	<0.05	0.16
9	17.9	20.5	0.5	<0.05	<0.05	0.13
11	18.1	19.8	0.6	<0.06	<0.05	0.11
13	21.5	12.9	0.6	<0.05	<0.05	0.12
15	18.5	5.6	0.6	<0.04	<0.05	<0.08
17	52.6	8.5	1.6	<0.07	<0.05	<0.14
19	37.9	5.4	1.0	<0.04	<0.05	<0.08
21	87.8	6.6	1.6	<0.05	<0.05	<0.10
23	100	7.8	1.6	<0.05	<0.05	<0.10
25	127	6.9	1.4	<0.05	<0.05	<0.11
27	137	8.1	1.3	<0.06	<0.05	<0.13

Table XVIII: Peeper 20 and 21 Ion Chromatography results, corrected for dilution

Cell	Chloride (mg Cl ⁻ L ⁻¹)	Sulfate (mg SO ₄ ²⁻)	Fluoride (mg F ⁻ L ⁻¹)	Phosphate (mg PO ₄ ³⁻ L ⁻¹)	Phosphate SRP (ppm)
0	0.49	3.72	0.06	<0.02	0.17
1	0.43	12.8	0.28	<0.11	0.10
3	0.41	13.5	0.29	<0.11	0.11
5	0.42	14.1	0.28	<0.11	0.12
7	0.48	18.6	0.29	<0.11	0.17
9	0.47	17.2	0.30	<0.11	0.60
11	0.49	16.7	0.27	0.123	0.70
13	0.48	14.9	0.28	<0.10	0.28
15	0.46	17.9	0.30	<0.12	0.28
17	0.48	18.5	0.28	<0.11	0.27
19	0.48	18.3	0.27	<0.11	0.05
21	0.47	18.3	0.28	<0.11	0.08
23	0.48	19.2	0.29	<0.11	0.23
25	0.48	18.9	0.30	<0.11	0.36
27	0.47	18.8	0.31	<0.12	0.16
Blank	NA	NA	NA	NA	NA
1ppm	NA	NA	NA	NA	1.11

Note: the following analytes were below detection limits, nitrite, nitrate, bromide.
Phosphate as SRP was measured using Hach reagents. 1ppm standard was only used for Phosphate SRP.

10. Appendix D: ICP-OES and ICP-MS

Table XIX: Peeper 18 and 19 ICP-OES, corrected for dilution

Cell	As (ppm)	B (ppm)	Ba (ppm)	Ca (ppm)	Fe (ppm)	K (ppm)	Mg (ppm)	Mn (ppm)	Na (ppm)	P (ppm)	Si (ppm)	Sr (ppm)
8	0.003	<0.06	0.046	34.8	0.150	3.04	9.11	0.09	13.0	0.10	12.2	0.211
4	0.004	<0.06	<0.045	31.7	0.015	3.23	8.67	0.01	12.9	<0.09	10.4	0.198
2	0.004	<0.06	0.046	32.6	0.014	3.15	8.68	0.01	12.7	<0.09	9.73	0.198
0	0.008	<0.06	0.058	38.4	0.051	3.37	9.81	0.09	13.1	<0.09	11.7	0.235
-2	0.005	<0.06	0.058	36.6	1.01	3.23	9.76	0.84	13.2	<0.09	13.6	0.229
-4	0.029	<0.06	0.085	36.7	8.14	3.48	9.64	0.78	13.4	0.541	14.5	0.240
-6	0.050	<0.06	0.121	37.9	10.9	3.79	9.76	0.81	13.4	1.27	14.8	0.255
-8	0.067	<0.06	0.145	47.6	15.6	4.92	12.0	1.07	16.1	1.40	16.5	0.328
-10	0.149	0.081	0.321	76.6	49.2	8.93	18.7	2.56	23.6	1.81	20.7	0.625
-12	0.145	0.100	0.431	98.4	65.0	11.8	25.6	3.46	30.4	1.69	22.5	0.813
-14	0.131	0.103	0.450	107	68.5	12.9	28.8	3.68	34.1	1.87	22.4	0.884
-16	0.125	0.105	0.472	114	73.9	13.7	30.6	3.81	37.2	1.96	22.3	0.947
-18	0.117	0.115	0.490	122	78.0	14.4	32.3	4.22	40.7	2.08	22.0	1.01
-20	0.109	0.113	0.507	132	79.8	14.7	34.2	4.94	45.0	2.10	21.5	1.06
-22	0.115	0.126	0.517	134	84.2	14.7	35.2	5.56	47.2	1.97	21.6	1.11
blank	< 0.2	<0.020	<0.015	0.017	<0.016	<0.067	<0.008	<0.015	0.02	<0.031	0.246	<0.015

Note: the following metals were below detection limit: Al, As, Be, Cd, Co, Cr, Cu, Li, Mo, Ni, Pb, Sb, Se, Ti, Tl, V, Zn; As was quantified with ICP-MS, not ICP-OES

Table XX: Peeper 20 and 21 ICP-OES, corrected for dilution

Cell	As (ppb)	Cu (ppm)	Ca (ppm)	Fe (ppm)	K (ppm)	Mg (ppm)	Mn (ppm)	Na (ppm)	P (ppm)	Si (ppm)	Sr (ppm)
8	0.97	<0.03	23.9	0.12	1.57	6.65	<0.03	0.21	<0.42	10.6	0.21
4	1.16	0.05	25.3	0.08	1.76	6.86	<0.03	0.13	<0.42	10.7	0.13
2	1.61	<0.03	25.6	0.08	1.63	7.02	0.04	0.25	<0.42	10.6	0.25
0	4.86	<0.03	24.8	0.11	1.72	6.10	2.24	0.28	<0.42	9.71	0.28
-2	13.0	<0.03	26.7	1.14	1.78	6.78	3.65	0.11	<0.42	10.9	0.11
-4	10.3	<0.03	30.6	4.04	2.06	7.63	4.49	0.13	0.24	12.3	0.13
-6	18.7	<0.03	30.9	3.30	2.06	7.59	4.71	0.17	0.14	12.3	0.17
-8	2.93	<0.03	29.0	3.97	2.07	7.21	3.55	0.12	0.32	12.1	0.12
-10	2.09	<0.03	22.3	0.46	1.78	5.84	1.80	0.27	0.05	9.92	0.27
-12	1.36	<0.03	21.7	0.27	1.71	5.55	1.20	0.14	<0.42	10.0	0.14
-14	1.84	<0.03	21.9	0.00	1.72	5.34	0.81	0.14	0.09	10.2	0.14
-16	4.89	<0.03	22.6	0.14	1.70	5.43	1.42	0.15	<0.42	10.5	0.15
-18	10.0	<0.03	23.7	0.78	1.85	5.53	2.64	0.11	0.13	11.1	0.11
-20	8.29	<0.03	25.8	3.00	1.77	5.67	4.02	0.29	0.13	12.0	0.29
-22	1.39	<0.03	24.9	2.67	1.92	5.30	4.37	0.30	0.04	11.9	0.30
blank	<0.06	<0.03	0.19	0.00	0.00	0.00	0.00	0.23	0.00	0.59	0.23

Note: The following elements were below the instrument detection limit: Cr, Arsenic was quantified using ICP-MS, 0.00 indicates below instrument detection limit.

Table XXI: peeper 22 and 23 ICP-OES results, corrected for dilution

Cell	As (ppm)	Fe (ppm)	Mn (ppm)	Pb (ppm)	Zn (ppm)
8	<0.31	50.7	3.66	<0.07	<0.01
4	<0.57	7.7	4.63	<0.14	0.19
2	<0.68	55.6	2.50	<0.17	0.24
0	<0.85	81.1	2.02	<0.21	<0.08
-2	<0.86	147	2.45	<0.21	<0.08
-4	0.96	221	2.84	<0.16	<0.06
-6	1.78	315	3.73	<0.22	<0.08
-8	1.72	285	3.31	<0.16	<0.06
-10	1.71	241	2.99	<0.2	<0.08
-12	<1.08	137	2.28	<0.26	<0.10
-14	0.74	154	1.99	<0.16	<0.06
-16	<1.25	94.1	1.78	<0.3	<0.12
-18	0.94	175	1.76	<0.12	<0.05
-20	0.95	184	1.89	<0.17	<0.07
-22	<1.02	191	2.16	<0.25	<0.09
blank	<0.1	<0.01	<0.01	<0.10	<0.09

Note: The number of analytes was decreased and limited to only As, Cu, Fe, Mn, Pb, Zn; Pb and Cu were below the instrument detection limit; the syringe used to sample peeper 23 had a zinc plunger, values may be lower than reported.

Table XXII: Peeper 20 and 21 ICP-MS results, corrected for dilution

Cell	7Li (µg/L)	11B (µg/L)	27Al (µg/L)	31P (µg/L)	*39K (µg/L)	*43Ca (mg/L)	51V (µg/L)	55Mn (µg/L)	56Fe (µg/L)	71Ga (µg/L)	75As (µg/L)	88Sr (µg/L)	98Mo (µg/L)	137Ba (µg/L)	238U (µg/L)
8	<1.4	11.0	26.0	<14.1	161	12.4	1.5	15.0	104	<1.4	1.2	222	2.0	14.4	0.5
4	<1.4	12.4	28.0	<14.1	171	12.8	1.5	11.3	64.7	<1.4	1.1	131	1.8	13.0	0.6
2	<1.4	14.8	18.6	<14.1	165	12.8	1.4	33.2	63.1	<1.4	1.1	260	2.8	15.9	0.6
0	6.1	14.9	<1.4	<14.1	182	12.7	<1.4	2.09x10 ³	84.5	1.6	1.7	301	17.3	22.1	1.3
-2	5.8	11.0	22.2	26.1	185	13.1	<1.4	3.21x10 ³	939	1.8	4.5	112	25.9	24.3	2.0
-4	<1.4	12.1	6.5	260	217	15.8	3.8	4.32x10 ³	3.73x10 ³	2.2	13.3	130	34.6	32.4	4.1
-6	7.1	12.7	10.0	129	196	15.1	4.0	4.14x10 ³	2.72x10 ³	2.2	11.0	173	41.5	30.7	4.0
-8	<1.4	12.0	17.7	310	201	14.3	6.1	3.24x10 ³	3.38x10 ³	2.6	17.6	127	42.6	35.7	2.6
-10	<1.4	14.9	<1.4	23.6	185	11.8	1.4	1.60x10 ³	411	1.9	3.0	281	34.0	27.1	<0.56
-12	<1.4	13.8	<1.4	16.0	181	11.2	<1.4	1.06x10 ³	217	1.6	2.1	149	37.1	23.0	<0.56
-14	5.9	14.1	<1.4	<14.1	182	11.4	<1.4	7.23x10 ²	23.1	1.4	1.3	146	43.8	20.6	<0.56
-16	6.2	14.5	<1.4	<14.1	183	11.7	<1.4	1.21x10 ³	117	1.6	2.0	154	44.7	21.9	<0.56
-18	6.4	13.4	<1.4	38.8	187	12.5	2.2	2.41x10 ³	688	1.7	4.8	119	49.4	23.5	0.9
-20	6.3	15.9	25.2	127	185	13.4	6.1	3.69x10 ³	2.59x10 ³	2.2	9.7	296	53.1	31.2	1.9
-22	6.7	14.6	56.8	103	180	13.0	4.8	3.95x10 ³	2.27x10 ³	2.2	8.5	307	54.8	32.5	1.8
blank	<0.5	16.5	<0.5	<5	<5	0.129	<0.5	<2	<5	<0.5	<0.2	232	<0.5	6.3	<0.2

Note: The following elements were below the instrument detection limit Be, Cr, Ni, Cu, Zn, Se, Nb, Pd, Ag, Sn, Sb, Cs, La, Ce, Pr, Nd, W, Tl, Th, Zr, Co.

*indicates analyte is normally quantified with ICP-OES

Table XXIII: Peeper 20 and 21 ICP-MS results, corrected for dilution cont.

Cell	238U (µg/L)	206Pb (µg/L)	207Pb (µg/L)	208Pb (µg/L)	51V (µg/L)	49Ti (µg/L)	85Rb (µg/L)	111Cd (µg/L)	90Zr (µg/L)	63Cu (µg/L)	59Co (µg/L)
8	0.5	<0.6	<0.6	<0.6	1.5	<1.4	<1.4	<0.6	<1.4	<2.0	<1.4
4	0.6	<0.6	<0.6	<0.6	1.5	<1.4	<1.4	<0.6	2.7	5.0	<1.4
2	0.6	<0.6	<0.6	<0.6	1.4	<1.4	<1.4	<0.6	<1.4	<2.0	<1.4
0	1.3	1.00	1.0	1.0	<1.4	<1.4	<1.4	<0.6	<1.4	<2.0	<1.4
-2	2.0	<0.6	<0.6	<0.6	<1.4	<1.4	1.4	<0.6	2.0	<2.0	1.4
-4	4.1	0.8	0.8	0.8	3.8	2.0	1.6	<0.6	<1.4	<2.0	1.6
-6	4.0	1.3	1.4	1.4	4.0	2.4	1.6	1.1	<1.4	<2.0	2.6
-8	2.6	0.9	0.9	1.0	6.1	2.7	1.7	<0.6	<1.4	<2.0	1.8
-10	<0.4	<0.6	<0.6	<0.6	1.4	<1.4	<1.4	<0.6	<1.4	<2.0	<1.4
-12	<0.6	<0.6	<0.6	<0.6	<1.4	<1.4	<1.4	<0.6	<1.4	<2.0	<1.4
-14	<0.6	<0.6	<0.6	<0.6	<1.4	<1.4	<1.4	<0.6	<1.4	<2.0	<1.4
-16	<0.6	<0.6	<0.6	<0.6	<1.4	<1.4	<1.4	<0.6	<1.4	<2.0	<1.4
-18	0.9	<0.6	<0.6	<0.6	2.1	<1.4	1.4	<0.6	<1.4	<2.0	<1.4
-20	1.9	<0.6	0.9	0.9	6.1	2.3	1.4	<0.6	<1.4	<2.0	1.7
-22	1.8	<0.6	0.9	0.8	4.8	2.2	<1.4	<0.6	<1.4	<2.0	1.7
blank	<0.2	<0.2	<0.2	<0.2	<0.5	<0.5	<0.5	<0.2	<1.4	<2.0	<1.4

Note: Note: The following elements were below the instrument detection limit Be, Cr, Ni, Zn, Se, Nb, Pd, Ag, Sn, Sb, Cs, La, Ce, Pr, Nd, W, Tl, Th, Zr. *indicates analyte is normally quantified with ICP-OES

Table XXIV: Peepers 18 and 19 ICP-MS results corrected for dilution

Cell	7Li (µg/L)	11B (µg/L)	27Al (µg/L)	*31P (µg/L)	*39K (µg/L)	*43Ca (mg/L)	51V (µg/L)	55Mn (µg/L)	56Fe (µg/L)	71Ga (µg/L)	75As (µg/L)	88Sr (µg/L)	98Mo (µg/L)	137Ba (µg/L)
8	14.7	27.4	6.09	<12	<12	<12	2.40	92.64	154	3.37	3.41	239	5.94	47.0
4	15.8	31.2	3.23	66.8	397	20.2	2.29	5.40	15.3	2.96	4.02	216	6.05	43.2
2	16.6	31.8	1.85	17.4	323	15.0	2.19	9.37	14.8	3.29	4.17	221	5.82	47.3
0	14.8	28.6	12.9	26.7	350	16.7	<1.5	92.1	51.5	4.25	7.58	266	4.79	62.1
-2	15.0	33.6	18.1	38.5	381	20.4	<1.5	922	977	4.36	5.30	266	4.86	64.4
-4	13.7	28.7	1.18	38.9	346	18.0	<1.5	826	6.78 x10 ³	6.09	28.8	269	4.40	89.7
-6	13.8	31.6	5.02	677	424	20.8	1.86	858	9.03 x10 ³	8.78	49.6	287	4.06	125
-8	13.2	31.0	2.37	1.29x10 ³	360	17.0	1.91	1.13x10 ³	13.0 x10 ³	10.4	66.7	373	3.67	155
-10	14.6	57.2	3.11	1.53x10 ³	533	24.3	3.50	2.69x10 ³	4.09 x10 ³	23.1	149	666	2.26	342
-12	15.9	72.9	3.98	1.98x10 ³	973	3.65	3.69	3.48x10 ³	51.2 x10 ³	30.5	145	831	1.79	442
-14	15.8	77.4	3.39	1.72x10 ³	1.18x10 ³	4.29	3.25	3.86x10 ³	55.4 x10 ³	31.8	131	900	<1.5	480
-16	16.8	79.8	3.33	2.11x10 ³	1.51x10 ³	5.42	2.93	4.04x10 ³	61.0 x10 ³	33.6	125	969	<1.5	495
-18	17.4	79.4	3.27	2.21x10 ³	1.55x10 ³	5.56	2.46	4.37x10 ³	63.39x10 ³	34.9	117	1.04x10 ³	<1.5	509
-20	17.7	80.1	4.38	1.91x10 ³	1.30x10 ³	4.92	2.08	5.10x10 ³	64.08x10 ³	36.3	109	1.09x10 ³	<1.5	511
-22	17.7	88.6	2.59	2.24x10 ³	1.59x10 ³	6.09	2.41	5.46x10 ³	65.1x10 ³	35.5	115	1.09x10 ³	1.42	512
blank	<0.5	4.62	<0.5	<5	<5	<5	<0.5	<2	<5	<0.5	<0.2	<1	<0.5	<1

Note: The following elements were below the instrument detection limit Be, Cr, Ni, Cu, Zn, Se, Nb, Pd, Ag, Sn, Sb, Cs, La, Ce, Pr, Nd, W, Tl, Th, Zr, Co.

*indicates analyte is normally quantified with ICP-OES

Table XXV: Peepers 18 and 19 ICP-MS, results corrected for dilution cont.

Cell	²³⁸ U (µg/L)	¹²¹ Sb (µg/L)	⁸⁵ Rb (µg/L)	⁸² Se (µg/L)	⁶³ Cu (µg/L)	⁶⁶ Zn (µg/L)	⁵² Cr (µg/L)	⁴⁹ Ti (µg/L)	⁹⁰ Zr (µg/L)	¹⁸² W (µg/L)
8	4.45	<0.6	<1.5	<0.6	3.04	7.59	<1.5	<1.5	<1.5	<0.6
4	4.78	<0.6	<1.5	<0.6	4.68	<3	<1.5	<1.5	<1.5	<0.6
2	4.97	<0.6	<1.5	<0.6	4.13	<3	<1.5	<1.5	<1.5	<0.6
0	3.64	17.05	<1.5	<0.6	4.05	12.03	<1.5	<1.5	<1.5	<0.6
-2	0.80	<0.6	<1.5	<0.6	<3	<3	<1.5	<1.5	<1.5	0.83
-4	0.61	<0.6	<1.5	<0.6	<3	<3	<1.5	<1.5	<1.5	1.14
-6	0.78	<0.6	<1.5	<0.6	<3	<3	<1.5	<1.5	<1.5	1.21
-8	0.62	<0.6	1.97	<0.6	<3	<3	<1.5	<1.5	<1.5	1.26
-10	<0.6	<0.6	3.82	<0.6	<3	<3	0.84	<1.5	1.76	1.11
-12	<0.6	0.59	4.78	<0.6	<3	<3	1.43	1.59	4.55	1.18
-14	<0.6	0.55	5.46	<0.6	<3	<3	1.33	1.38	1.47	0.90
-16	<0.6	0.60	6.08	<0.6	<3	<3	1.45	<1.5	<1.5	0.75
-18	<0.6	0.63	6.55	1.20	<3	<3	1.43	<1.5	<1.5	<0.6
-20	<0.6	0.63	6.80	1.04	<3	<3	1.47	<1.5	<1.5	0.52
-22	<0.6	0.79	6.75	1.47	<3	<3	1.13	<1.5	3.37	0.74
blank	<0.2	<0.2	<0.5	<0.2	<1	<1	<0.2	<0.5	<0.5	<0.2

Note: The following elements were below the instrument detection limit. Be, Ni, Zn, Nb, Pd, Ag, Sn, Cs, La, Ce, Pr, Nd, Tl, Th, Co

*indicates analyte is normally quantified with ICP-OES

11. Appendix E: Surface water data

Table XXVI: Surface water samples between sites (September 18th, 2020)

Site ID	Site number	Distance downstream (km)	pH	Temp (C°)	ORP (mV)	SC (µS/cm)	Alkalinity (CaCO ₃ mg L ⁻¹)	DIC (mg C L ⁻¹)	Std. Dev‰	δ ¹³ C-DIC ‰ VPDB	Std Dev. ‰ VPDB
Historical	BTC-0	0	6.42	15.9	-180	741	60.2	bdl	0.14	-20.2	0.11
BMS	BTC-1	1.30	7.69	6.87	254	257	87.4	27.4	1.49	-9.4	0.18
Private drive	BTC-2	1.61	7.53	7.37	258	227	100	23.5	0.70	-9.1	0.05
Picnic area	BTC-3	2.75	8.19	7.82	265	196	77.0	19.8	0.87	-7.4	0.07
Thompson Park	BTC-4	4.36	8.08	8.55	282	212	77.8	18.1	1.29	-7.1	0.14
Blacktail loop	BTC-5	13.2	7.11	14.4	157	364	84.0	21.8	0.78	-11.6	0.12
Three Bears	BTC-6	15.0	8.00	12.4	229	282	72.6	19.0	0.81	-9.7	0.18
Father Sheehan	BTC-7	18.3	7.94	11.1	268	325	85.0	22.2	0.92	-11.7	0.12
KOA	BTC-8	20.8	8.26	12.0	278	390	81.2	25.6	0.70	-11.6	0.03
Slag Canyon	BTC-9	21.4	7.95	14.1	269	1731	64.2	16.6	0.50	-9.0	0.10
Santa Clause	BTC-10	24.9	8.14	14.9	297	1452	81.0	20.6	1.17	-10.5	0.35

12. Appendix F: Groundwater wells



Figure 30: Groundwater wells sampled in BMS site Stemp_3 (left) and SW_UFLCW (right).



Figure 31: Groundwater well sampled in BMS site Stemp_1

13. Appendix G: Surface Water Field Photos



Figure 32: BTC-6 surface water site



Figure 33: BTC-7 Surface water site



Figure 34: BTC-8 surface water site



Figure 35: BTC-3 surface water site



Figure 36: BTC-4 surface water site

SIGNATURE PAGE

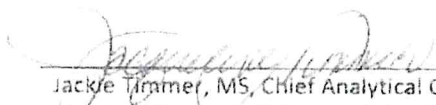
This is to certify that the thesis prepared by Kyle M. Nacey entitled "Comparison of Pore Water Chemistry Between an Upland Restoration Site and a Valley Superfund Site using Dissolved Inorganic Carbon Isotopes Along Blacktail Creek, Butte, MT" has been examined and approved for acceptance by the Department of Geological Engineering, Montana Technological University, on this 4th day of May, 2021.



Glenn Shaw, PhD, Professor and Department Head
Department of Geological Engineering
Chair, Examination Committee



Christopher H. Gammons, PhD, Professor
Department of Geological Engineering
Member, Examination Committee



Jackie Timmer, MS, Chief Analytical Chemist
Montana Bureau of Mines and Geology
Member, Examination Committee



Beverly Hartline, PhD
Professor *Emerita*
Member, Examination Committee